ACADEMIA
NANO: SCIENCE,
MATERIALS, TECHNOLOGY

Review Article
Published: 2025-07-31
https://doi.org/10.20935/AcadNano7835

# Nanofiller modifications for boosting piezoelectric performance in lead-free polymer nanocomposites

Jong Moon Lee[1,2], Hung-Vu Tran[1,2,3,4], Pailinrut Chinwangso[1,2], T. Randall Lee[1,2,*]

Academic Editor: Haiyang Zou

## Abstract

Piezoelectric polymer nanocomposites have attracted substantial interest due to their capability to combine the excellent piezoelectric properties of ceramics with the flexibility of polymers. This combination makes them highly suitable for applications in portable and wearable sensors, as well as energy harvesters. However, their performance is often hindered by inconsistent local piezoelectricity, which results from uneven nanofiller distribution and ineffective stress transfer at the nanofiller/polymer interfaces. Addressing these challenges necessitates improving the dispersibility of nanofillers and enhancing interfacial interactions between nanofillers and the polymer matrix. Additionally, increasing and/or arranging spontaneous polarization in nanofillers can enhance the overall piezoelectricity of nanocomposites, mitigating performance declines. Recent studies aimed at improving the performance of lead-free piezoelectric polymer nanocomposites through nanofiller modifications such as surface coating/decoration and chemical doping have been summarized. The proposed modes of performance enhancement by surface-coated and chemically doped nanofillers have been introduced and summarized. Finally, some suggestions and strategies for future research endeavors are presented.

**Keywords:** *piezoelectricity, polymer nanocomposite, surface coating, chemical doping*

**Citation:** Lee JM, Tran H-V, Chinwangso P, Lee TR. Nanofiller modifications for boosting piezoelectric performance in lead-free polymer nanocomposites. *Academia Nano: Science, Materials, Technology* 2025;2. https://doi.org/10.20935/AcadNano7835

## 1. Introduction

As global energy demand continues to rise, the development and commercialization of reliable alternative energy sources have become increasingly desirable to diversify the energy supply and reduce the risks associated with fossil-fuel dependence. In addition to power generation from renewable sources such as solar, wind, hydro, geothermal, and biomass, energy harvesting has emerged as a promising technology for generating electricity, particularly for powering portable, wearable, or remotely controlled devices. These technologies harness ambient energy sources in the form of pressure, vibration, and heat generated from the human body, buildings, and other structures [1, 2]. Various energy-harvesting processes utilize these ambient energy sources, including photovoltaics, which generate electricity from ambient light [3, 4]; pyroelectricity, which produces electrical charges in response to temperature changes [5, 6]; triboelectricity, which generates electrical charges through contact and friction between different materials [7–9]; electromagnetism, which converts magnetic field induced by vibration energy into electrical power [10, 11]; electrochemical reactions driven by humidity or strain to generate electrical energy [12–17]; and piezoelectricity, which generates electricity from mechanical stress.

Piezoelectricity has been widely studied due to its unique ability to convert mechanical energy directly into electricity (the direct piezoelectric effect). Mechanical stress applied to a piezoelectric material deforms the non-centrosymmetric crystal lattice of the material. This deformation displaces the positive and negative charge centers within the material, creating an electric polarization and leading to an accumulation of electrical charge on the surfaces of the material, which can be collected and used to generate electricity [18, 19]. Polarization (electric displacement) and stress can be related through the piezoelectric coefficient as expressed in **Equation (1)**,

$$P_i = d_{ijk} \cdot \sigma_{jk} \quad (1)$$

where $P$ is the polarization (first-rank tensor), $d$ is the piezoelectric coefficient (third-rank tensor), $\sigma$ is the stress (second-rank tensor), $i$ is the direction of polarization, $j$ is the direction of the plane perpendicular to the applied force, and $k$ is the direction of the applied force.

The nine stress tensor components in Cartesian coordinates (**Figure 1a**) can be expressed as a 3 × 3 matrix in **Equation (2)**. The stress tensor becomes symmetric ($\sigma jk = \sigma kj$), assuming angular momentum equilibrium, meaning the object does not rotate about any axis when the force is applied. The order of the stress tensor can be reduced using Voigt notation.

$$\sigma_{jk} = \begin{bmatrix} \sigma_{11} & \sigma_{12} & \sigma_{13} \\ \sigma_{21} & \sigma_{22} & \sigma_{23} \\ \sigma_{31} & \sigma_{32} & \sigma_{33} \end{bmatrix} = \begin{bmatrix} \sigma_{11} & \sigma_{12} & \sigma_{13} \\ \sigma_{21} & \sigma_{22} & \sigma_{23} \\ \sigma_{31} & \sigma_{32} & \sigma_{33} \end{bmatrix} \rightarrow \sigma_j = \begin{bmatrix} \sigma_1 & \sigma_6 & \sigma_5 \\ & \sigma_2 & \sigma_4 \\ & & \sigma_3 \end{bmatrix}$$

angular momentum equilibrium ($\sigma_{jk} = \sigma_{kj}$) Voigt notation (2)

[1]Department of Chemistry, University of Houston, Houston, TX, USA.
[2]The Texas Center for Superconductivity, University of Houston, Houston, TX, USA.
[3]NTT Hi-Tech Institute, Nguyen Tat Thanh University, Ho Chi Minh City, Vietnam.
[4]Center for Hi-Tech Development, Nguyen Tat Thanh University, Saigon Hi-Tech Park, Ho Chi Minh City, Vietnam.
*email: trlee@uh.edu

The reduced equation and its matrix form are shown in **Equation (3)**, which is widely used in materials science and engineering.

$$Pi = d_{ij}\sigma_j \rightarrow \begin{bmatrix} P_1 \\ P_2 \\ P_3 \end{bmatrix} = \begin{bmatrix} d_{11} & d_{12} & d_{13}d_{14} & d_{15} & d_{16} \\ d_{21} & d_{22} & d_{23}d_{24} & d_{25} & d_{26} \\ d_{31} & d_{32} & d_{33}d_{34} & d_{35} & d_{36} \end{bmatrix} \begin{bmatrix} \sigma_1 \\ \sigma_2 \\ \sigma_3 \\ \sigma_4 \\ \sigma_5 \\ \sigma_6 \end{bmatrix} \quad (3)$$

Among the piezoelectric coefficients, $d_{33}$ and $d_{31}$ are particularly significant especially for thin films. The coefficient $d_{33}$ represents the longitudinal mode, where the polarization is generated in the same direction as the applied mechanical stress, such as compression (**Figure 1b**). In contrast, $d_{31}$ represents the transverse mode, where the polarization is generated perpendicular to the applied mechanical stress such as during bending or stretching (**Figure 1c**).

For a material to exhibit piezoelectricity, its crystal structure must be non-centrosymmetric, lacking an inversion center. The operation matrix for inversion ($i$) shows that, after inversion, the polarization in one direction becomes equal to its negative counterpart as shown in **Equation (4)**. Given that the applied stress is nonzero, the piezoelectric coefficient must be zero to satisfy this condition. Consequently, centrosymmetric materials cannot exhibit piezoelectricity [18–20].

$$\begin{bmatrix} P_1 \\ P_2 \\ P_3 \end{bmatrix} = \begin{bmatrix} -1 & 0 & 0 \\ 0 & -1 & 0 \\ 0 & 0 & -1 \end{bmatrix} \begin{bmatrix} P_1 \\ P_2 \\ P_3 \end{bmatrix} \rightarrow \quad (4)$$
$$P_i = -P_i \rightarrow d_{ij}\,\sigma_j = -d_{ij}\,\sigma_j \rightarrow d_{ij} = -d_{ij} = 0$$

The $d_{33}$ and $d_{31}$ piezoelectric modes are preferred in energy harvesting applications due to their high electromechanical coupling efficiency, mechanical simplicity, and compatibility with conventional device geometries such as cantilevers, membranes, and films. These modes involve normal or longitudinal strains, which can be efficiently generated under common mechanical stimuli with vertical poling procedures that simplify fabrication. In contrast, modes corresponding to transverse shear deformation, such as $d_{15}$, require more complex device structures and poling configurations, and their energy conversion efficiency is typically lower [21]. Thus, while $d_{15}$ may be useful in specialized cases, $d_{33}$ and $d_{31}$ remain the most practical and effective modes for evaluating and utilizing piezoelectric performance in energy harvesting devices.

Piezoelectric materials can harness common biomechanical movements such as walking, running, and pulsations, as well as ambient mechanical vibrations from machinery, buildings, and other structures. This versatility makes them suitable for various applications. In addition, piezoelectric devices are often simple in construction and can be miniaturized, which is advantageous for the development of compact and lightweight energy-harvesting systems. Depending on the synthesis strategy used, piezoelectric materials can give high energy densities [22–27].

In general, inorganic piezoelectric materials such as lead zirconate titanate ($Pb[Zr_xTi_{1-x}]O_3$, PZT) and barium titanate ($BaTiO_3$, BTO) exhibit high piezoelectric properties and thermal stability, making them excellent candidates for a wide range of applications [18, 28–30]. However, their rigidity and brittleness make them unsuitable for applications requiring flexibility. Additionally, some inorganic materials, particularly those containing lead (e.g., PZT), pose environmental toxicity concerns, rendering them unsuitable for wearable or implantable devices despite their excellent piezoelectric performance [22, 30].

To address these limitations, significant attention has been directed toward piezoelectric polymers such as poly(vinylidene fluoride) (PVDF) and its copolymers. These polymers are lightweight, flexible, biocompatible, and easy to process [30]. However, their piezoelectric performance does not match that of inorganic counterparts [28]. Therefore, flexible piezoelectric nanocomposites consisting of a polymer matrix with dispersed inorganic nanofillers have been extensively investigated to combine the benefits of both material types [18, 23, 25–29, 31].

Numerous studies have explored the incorporation of various inorganic nanofillers, such as perovskites (e.g., PZT, BTO) [32, 33], carbon materials (e.g., carbon nanotubes, nanodiamonds, carbon black) [34–36], semiconductors (e.g., ZnO, GeSe, ZnSe, $SnO_2$) [37–40], and salts (e.g., ammonium, nitrate salts) [41, 42] into polymer matrices to enhance the piezoelectric properties of flexible nanocomposites. The improved piezoelectric performance arises not only from the inherent piezoelectric properties of the nanofillers but also from the increase in electroactive phases of the polymers induced by highly polarized and charged nanofillers [43, 44]. However, performance enhancement can be limited by local deviations in piezoelectricity, primarily due to the uneven distribution of nanofillers within the polymer matrix and inefficient stress transfer at nanofiller/polymer interfaces. These issues are often exacerbated by high internal resistance and poor interaction between the nanofillers and the polymer matrix [45].

Addressing these challenges involves either enhancing the piezoelectric properties of the nanofillers to offset performance losses or improving the interfacial interaction between nanofillers and the polymer matrix, which can lead to a higher electrical potential for a given stress. With these considerations, recent research efforts aimed at enhancing the piezoelectric performance of lead-free nanocomposites through nanofiller modifications have been highlighted, as summarized in **Figure 2**, specifically for energy-harvesting and sensing applications.

Modifications of nanofillers can be reliably confirmed using a range of instrumental analytical techniques that provide insight into structural, compositional, and surface chemical changes. In the case of surface coatings, most studies have employed scanning electron microscopy (SEM) and/or transmission electron microscopy (TEM) to directly visualize morphological changes, and Fourier-transform infrared spectroscopy (FT-IR) to verify the presence of new functional groups and surface chemical modifications. X-ray diffraction (XRD), on the other hand, typically does not show distinct changes resulting from surface modification but remains effective for confirming the presence of nanofillers in the composites. Additionally, FT-IR is used to demonstrate enhanced β-phase formation in PVDF upon nanofiller incorporation, as indicated by increased peak intensities. A few studies have also utilized phase-field simulations to intuitively visualize enhanced stress transfer efficiency and improved piezoelectric properties resulting from surface modification, whereas most studies explained these improvements based solely on enhanced output performance [46]. In the case of doping, the presence of dopants is commonly confirmed by peak shifts in XRD and elemental analysis using energy-dispersive X-ray spectroscopy (EDS) [47]. Some exemplary datasets illustrating these techniques are shown in **Figure 3**.

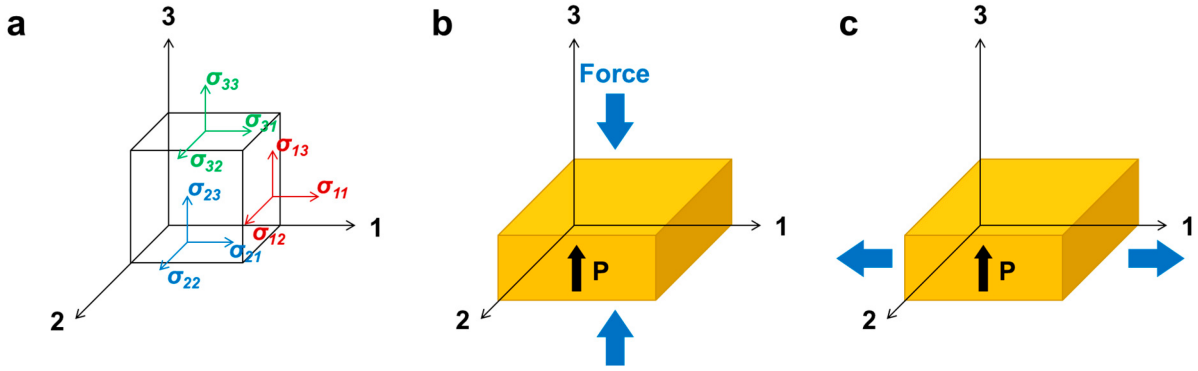


**Figure 1** • (**a**) Nine stress tensor components in Cartesian coordinates. (**b**) Longitudinal mode ($d33$): Polarization along the 3-axis generated by an applied force along the 3-axis. (**c**) Transverse mode ($d31$): Polarization along the 1-axis generated by an applied force along the 3-axis.

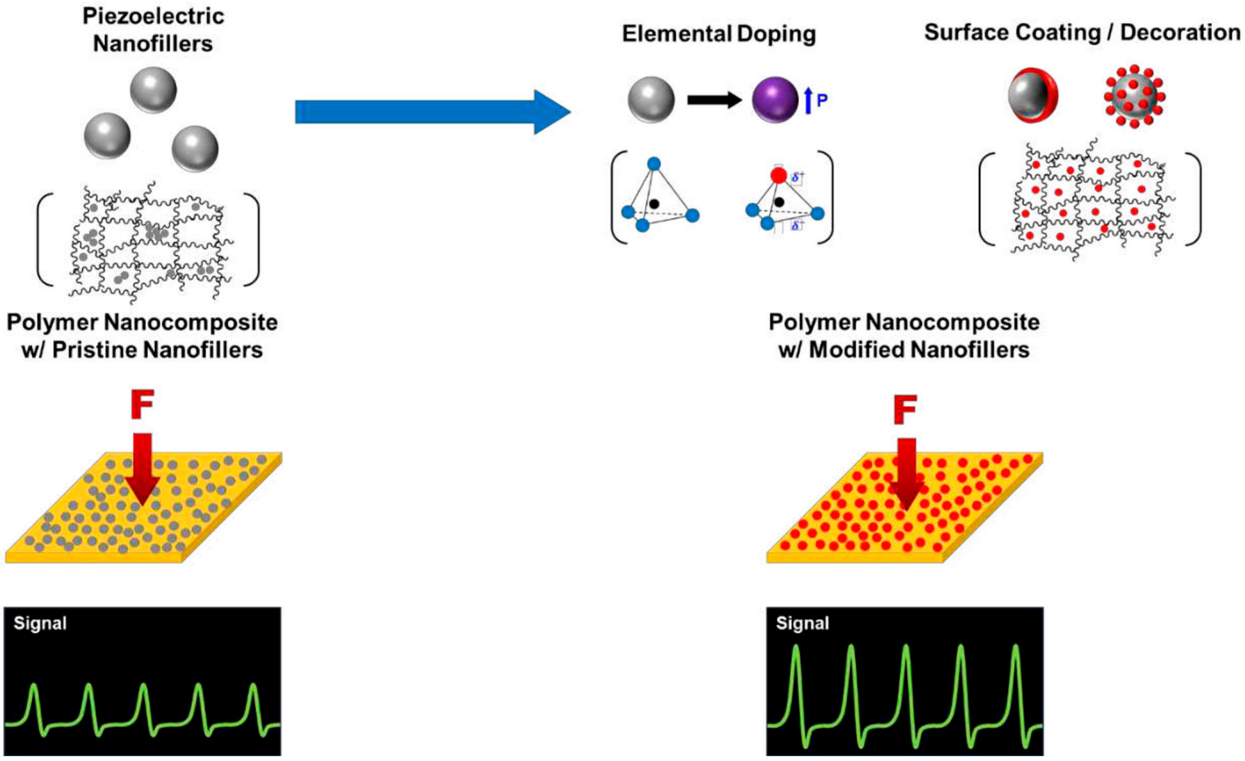


**Figure 2** • Overview of nanofiller modification strategies for boosting piezoelectric performance of polymer nanocomposites.

## 2. Coating of nanofillers

The primary purpose of applying a shell layer on homogeneous nanofillers is to enhance their compatibility and dispersibility within polymer matrices. Inorganic nanofillers often exhibit poor compatibility with polymer matrices and tend to aggregate due to their high surface energy. These issues can lead to inefficient stress transfer at the interface and non-uniform distribution of nanofillers, ultimately diminishing piezoelectric performance [48]. This chapter explores recent surface coating approaches to address these challenges. For clarity, surface-coated nanofillers will be consistently referred to as "core@shell" throughout this article. Any different terminology found in the cited references will be adapted to this convention to avoid confusion.

### 2.1. Coating of nanofillers with PDA

Polydopamine (PDA) has been extensively used as a coating layer, particularly when the polymer matrix is PVDF or its copolymer [46, 49–55]. One of the most common types is the BTO@PDA nanofiller, chosen for its simplicity and ease of preparation. This involves dispersing BTO nanoparticles in a Tris-HCl buffer solution followed by the addition of dopamine hydrochloride (**Figure 4a**) [46, 49–53]. During the in situ polymerization of PDA, catechol groups are grafted onto the surface of BTO, forming a stable PDA layer on the nanoparticles [56, 57]. Amine groups on the PDA surface can form hydrogen bonds with -CF2 groups in PVDF chains, thereby promoting the alignment of polymer segments into the β-phase conformation during crystallization and enhancing interfacial interactions [56]. The resulting BTO@PDA nanoparticles exhibited improved dispersibility and compatibility

within the PVDF matrix, as the PDA layer prevents nanoparticle agglomeration and introduces functional groups that enable strong interfacial interactions with the polymer chains [58]. For instance, pressure sensors were prepared by casting a mixture of BTO@PDA nanoparticles and PVDF solution, followed by poling—a process that aligns randomly oriented dipoles in the material by applying a strong electric field [49]. The BTO@PDA/PVDF composite film exhibited an output voltage of 9.3 V under an impact force of 12 N at 1 Hz, outperforming the BTO/PVDF film (4.7 V) due to the homogeneous dispersion of BTO@PDA nanoparticles, which led to fewer defects at the interface with the PVDF matrix. Alternatively, electrospinning—a method that uses electric force to draw charged threads from polymer solutions—was used to produce BTO@PDA/PVDF composite fibers [50]. The BTO@PDA/PVDF composite fiber-based sensor showed a sensitivity of 3.95 V/N within a 0.07–3 N range, significantly surpassing that of BTO/PVDF fibers (2.26 V/N) under the same conditions. This improvement was theoretically supported by a comprehensive phase-field simulation based on a Fourier spectral iterative perturbation method, which predicted the distributions of stress, electric field, and piezoelectric potential under an external stress of 1 MPa. The function of PDA was illustrated through a "muscle fiber" analogy (**Figure 4b**). Just as the connective tissue surrounding muscle fibers uniformly transfers external stress and enhances the mechanical strength of muscle tissues, PDA surrounding BTO nanoparticles serves a similar role by forming strong interfacial bonds between nanofillers and the polymer matrix. The BTO@PDA/PVDF system was further investigated by varying the amount of PDA during the BTO coating process. It was found that the β-phase content in PVDF, which is closely related to the piezoelectric output voltage, increased with the PDA volume fraction up to 2.15%, corresponding to a PDA layer thickness of ~20 nm [46]. At this PDA layer thickness, the interaction between the partially positively hydrogens in the amine groups of PDA and the negatively polarized -$CF_2$ groups of PVDF promoted the formation of the all-trans conformation (β-phase) in PVDF under the presence of a high electric field during the electrospinning process, thereby enhancing its piezoelectric properties.

A different approach was adopted by anchoring BTO@PDA nanoparticles onto the surface of electrospun poly(vinylidene- trifluoroethylene) (PVDF-TrFE) fibers instead of embedding them. A "hierarchical micro-structured" membrane was created by immersing pristine PVDF-TrFE nanofiber mats in aqueous dispersions of BTO@PDA nanoparticles, followed by the application of ultrasonication to firmly anchor the nanoparticles onto the nanofibers [51]. For comparison, membranes were also produced in a conventional way, where BTO@PDA nanoparticles were directly incorporated into the PVDF-TrFE solution prior to the electrospinning process. The piezoelectric nanogenerators (PENGs) prepared from BTO/PVDF-TrFE, BTO@PDA/PVDF-TrFE, and BTO@PDA-anchored PVDF-TrFE nanofiber mats produced output voltages of 1.85 V, 2.28 V, and 3.1 V, respectively, under a 700 N load at 2 Hz. The enhanced performance of the BTO@PDA-anchored PVDF-TrFE nanofibers was attributed to the PDA coating, which led to a reduction in fiber defects and improved stress transfer at the nanoparticle/polymer interface. These improvements facilitate more efficient piezoelectric responses by ensuring that mechanical stress is more effectively converted into electrical energy. Furthermore, when the impact frequency was increased from 2 Hz to 3 Hz, the hierarchical micro-structured membrane achieved a maximum output voltage of 6 V and a current of 1.52 μA.

To overcome the low piezoelectricity of natural cellulose while taking advantage of its eco-friendly and low-cost characteristics, BTO@PDA nanoparticles were incorporated into cellulose nanofibers (CNFs) for the development of PENGs [52]. The BTO@PDA-loaded CNF membrane was prepared by uniformly mixing BTO@PDA nanoparticles into CNF aqueous suspensions with ultrasonication. This membrane was then combined with a layer of electrospun maleic anhydride grafted PVDF (PVDF-g-MA) nanofibers to create a bilayer structure. The presence of PDA facilitated a strong interfacial interaction with cellulose, thereby enhancing nanoparticle dispersion and preventing their aggregation. Moreover, the mechanical strength and durability of the bilayer membrane were significantly improved through a chemical coupling reaction between the amine groups of PDA and the maleic anhydride units in PVDF-g-MA. This bilayered PENG generated a maximum output voltage of 3.2 V and current of 0.25 μA under a 5 N load at 3 Hz.

The piezoelectric sensitivity of electrospun PVDF-TrFE was enhanced by incorporating BTO@PDA nanowires with a high aspect ratio [53]. This approach afforded coaxial composite nanofibers that respond more effectively to external mechanical loads. The PDA coating on the BTO nanowires not only improved the nanofiller/polymer interfacial interaction but also promoted the β-phase in PVDF-TrFE, significantly increasing the piezoelectric response (**Figure 4c**). Consequently, this composite achieved a piezoelectric output voltage of 18.2 V and a current of 1.5 μA under an impact force of 5 N at 1 Hz, outperforming spherical BTO@PDA nanoparticle-based PENGs, which produced 7.5 V and 0.4 μA. Notably, the inclusion of BTO@PDA nanowires made the PENGs more responsive (4.3 V/N) compared to their BTO@PDA nanoparticle counterparts (2.3 V/N), especially at lower forces (<1.5 N), which is suitable for sensing subtle biomechanical movements. This remarkable performance advantage was supported by COMSOL simulations, which revealed that piezoceramic materials with one-dimensional (1D) nanowire structures exhibit greater strain responsiveness and more effective stress transfer along the axial direction of the fiber than their zero-dimensional (0D) nanoparticle counterparts.

Self-poled and bio-flexible PENGs were developed using Ca, Zr co-doped BTO ($Ba_{0.85}Ca_{0.15}Zr_{0.10}Ti_{0.90}O_3$, BCZT) nanoparticles embedded in a polylactic acid (PLA) biopolymer matrix [54]. PLA stands out in energy harvesting applications alongside PVDF for its biodegradability, biocompatibility, and inherent piezoelectricity, which does not require external poling due to the polarity induced by the carbonyl groups branching out from its backbone [58, 59]. The BCZT@PDA/PLA nanocomposite film prepared by solution casting produced an output voltage and current of 14.4 V and 0.55 μA, respectively, under finger tapping (~1.8 N at 0.3 Hz). Later, Zr-doped hydrogen trititanate ($H_2(Zr_{0.1}Ti_{0.9})_3O_7$, HZTO) was also incorporated in the form of HZTO@PDA nanowires into the PLA matrix [55]. Interestingly, the local piezoelectric constant ($d_{33}$) of the synthesized HZTO nanowire obtained using piezoresponse force microscopy (PFM) reached 26 pC/N, which is comparable to that of BTO nanowires (~20 pC/N) [60]. Note that $d_{33}$ is obtained by the ratio of the amplitude in the z-direction to the applied voltage in the z-direction. The unit of $d_{33}$, pm/V, reported in the original reference was converted to pC/N for consistency. The PENGs based on HZTO@PDA/PLA film generated an output voltage and a current of 5.41 V and 0.26 μA, respectively, through finger tapping (~2 N).

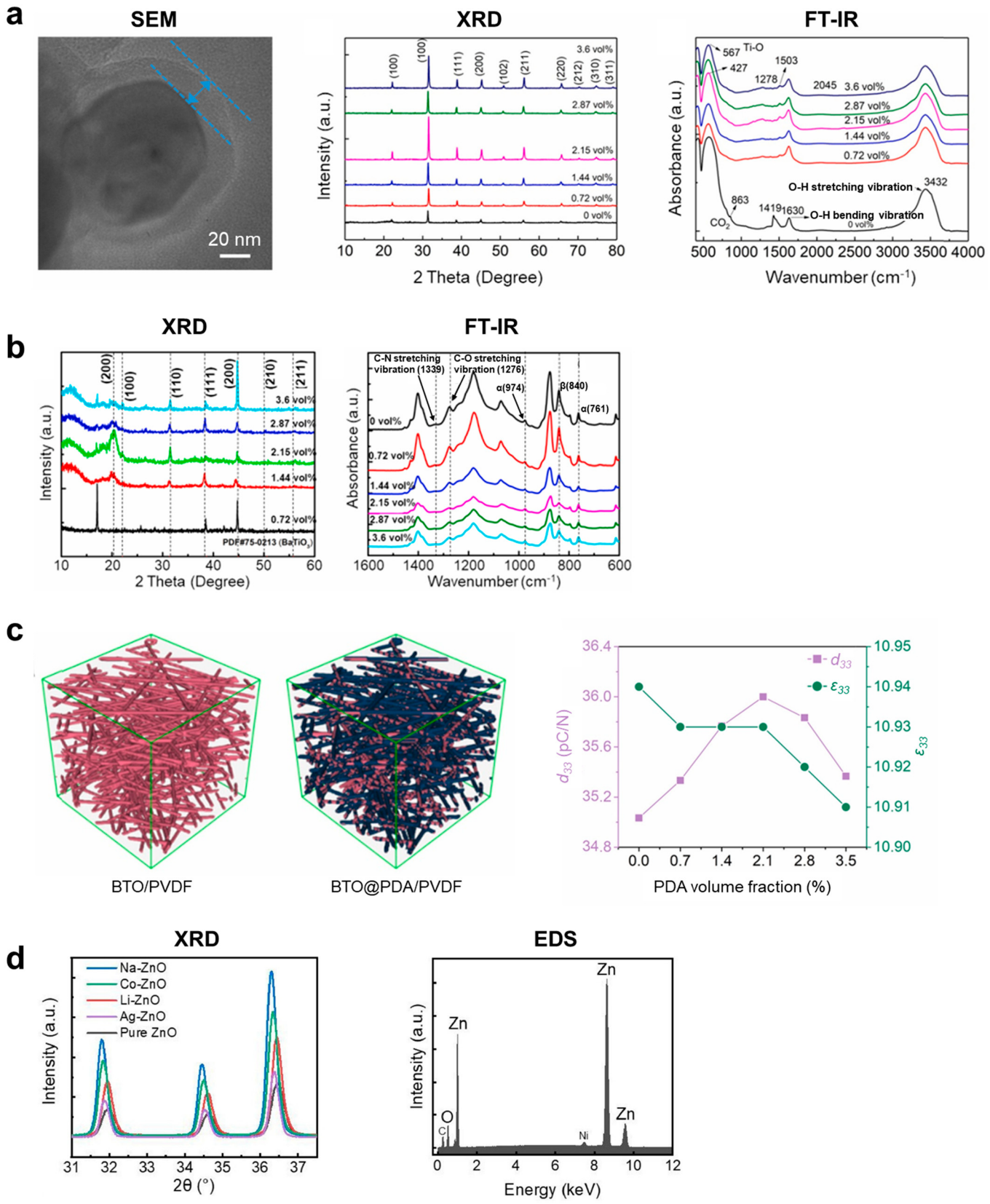


**Figure 3** • Representative characterization data confirming nanofiller modification and its effect on the piezoelectricity of nanocomposites. (**a**) SEM, XRD, and FT-IR data of BTO nanoparticles coated with varying volume fractions of PDA (0, 0.72, 1.44, 2.15, 2.87, and 3.6%). (**b**) XRD and FT-IR data of BTO/PVDF nanocomposites incorporating BTO nanoparticles with different PDA coating levels. (**c**) Visualized structural modeling of BTO/PVDF nanocomposites using phase-field simulations based on unmodified and PDA-coated BTO nanoparticles, along with the calculated piezoelectric coefficient ($d_{33}$) and stiffness coefficient ($\varepsilon_{33}$) at varying PDA concentrations. Reproduced with permission from [46]. Copyright 2021, Elsevier. (**d**) XRD and EDS data of metal-doped ZnO nanoparticles. Reproduced with permission from [47]. Copyright 2020, Elsevier.

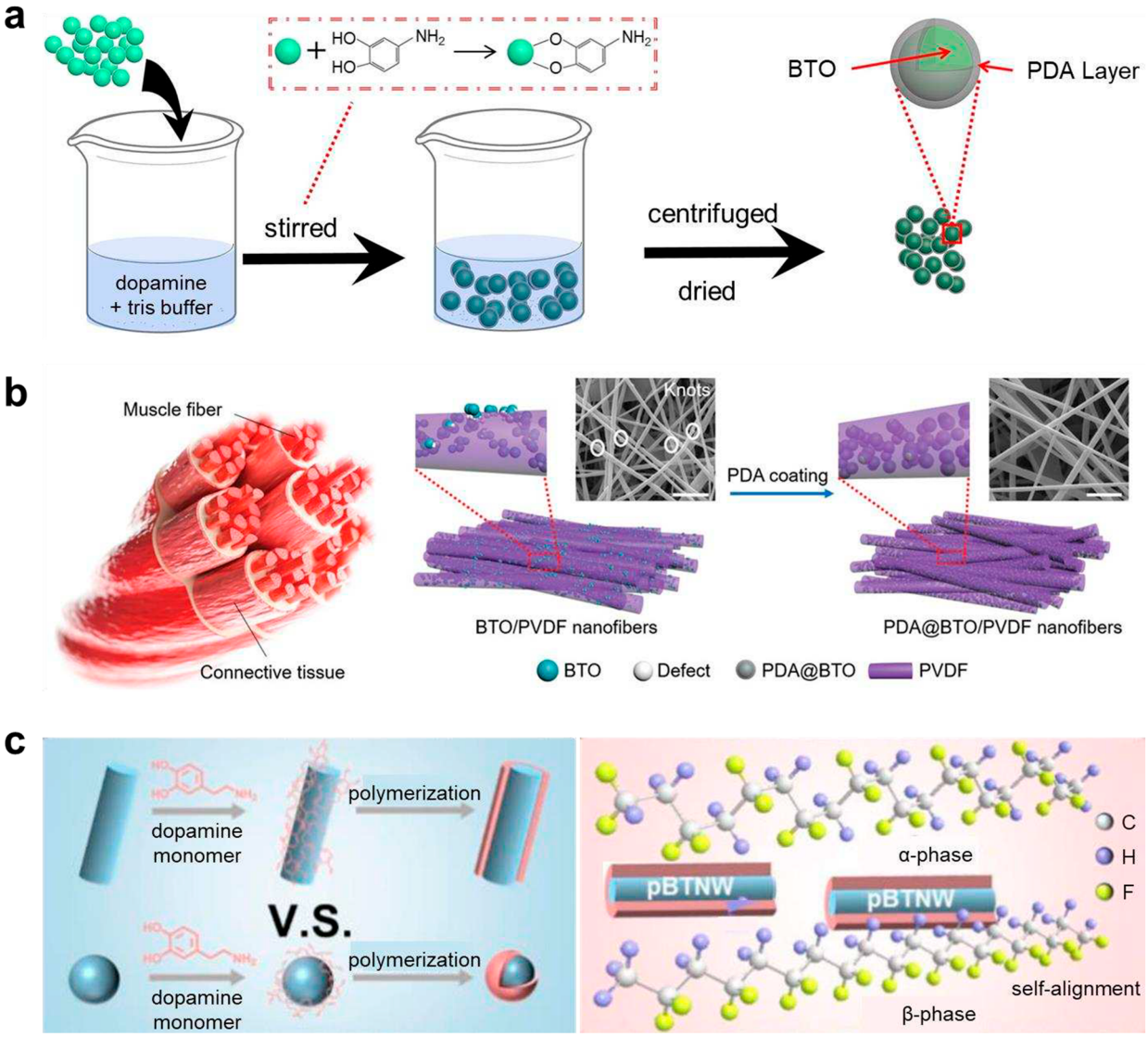


**Figure 4** • BTO@PDA nanofillers. (**a**) Coating BTO nanoparticles with PDA. Reproduced with permission from [49]. Copyright 2020, Elsevier. (**b**) Enhanced compatibility between BTO@PDA nanoparticles and PVDF nanofibers where PDA functions similarly to connective tissue in muscle fiber structures. Reproduced with permission from [50]. Copyright 2021, Wiley-VCH. (**c**) Enhanced β-phase in PVDF induced by BTO@PDA nanowires. Reproduced with permission from [53]. Copyright 2022, Elsevier.

PDA is widely used to modify piezoelectric nanofillers due to its strong adhesion, enabling uniform coverage across various materials and improving dispersion and stress transfer in polymer matrices. The catechol and amine groups in PDA promote interfacial interactions, facilitating β-phase formation in PVDF and enhancing piezoelectric performance. However, challenges such as potential insulating effects at high PDA content and variability in polymerization conditions can hinder polarization and affect reproducibility, respectively [46, 61]. Therefore, optimizing the coating process to achieve precise thickness control is critical.

### 2.2. Coating of nanofillers with other polymers

While not as common as PDA, there are several other polymers that have been used to coat nanofillers and enhance the piezoelectric performance of composites. One approach explored the use of PVDF-TrFE as a coating layer for BTO to improve the dispersion of nanoparticles within a polymer matrix of the same material [62]. The BTO@PVDF-TrFE nanoparticles were prepared using the nonsolvent-induced phase separation (NIPS) method. This process involved dispersing BTO nanoparticles in a PVDF-TrFE/DMF solution, followed by the addition of the non-solvent, 1-octanol (**Figure 5b**). The BTO@PVDF-TrFE/PVDF-TrFE nanocomposite film achieved a maximum output voltage and current of 59.5 V and 6.52 μA, respectively, under a 100 N load at 2.5 Hz. Notably, these values were 4.8 times and 2 times higher, respectively, compared to those of uncoated BTO/PVDF-TrFE films, demonstrating the impact of improved nanoparticle dispersibility in the matrix.

Surface-initiated polymerization was employed to graft a layer of polymethylmethacrylate (PMMA) on the surface of BTO nanowires, aiming to improve the dispersion of nanofillers and the interfacial interaction between BTO nanowires and the PVDF-TrFE matrix (**Figure 5a**) [63]. BTO nanowires were first hydroxylated with $H_2O_2$, then functionalized with γ-aminopropyl triethoxysilane (γ-APS), and subsequently treated with α-bromoisobutyryl bromide (BIBB) to provide initiator sites, enabling the atomic transfer radical polymerization (ATRP) of MMA and the formation of covalently grafted PMMA shells. The

electrospun BTO@PMMA/PVDF-TrFE nanocomposite achieved 12.6 V and 1.30 μA when subjected to a 4 mm displacement by bending at 2 Hz. In contrast, the composite prepared with unmodified BTO nanowires reached 8 V and 0.9 μA, respectively.

Zinc sulfide (ZnS) microspheres coated with polyaniline (PANI) were incorporated into poly(vinylidene fluoride- hexafluoropropylene) (PVDF-HFP) (**Figure 5c**) [64]. During the polymerization, PANI exists in its protonated form (emeraldine salt) under acidic conditions, allowing the positively charged -NH+ groups to interact electrostatically with negatively charged or polar sites on the ZnS surface [65]. The electrospun ZnS@PANI/PVDF-HFP composite achieved a maximum output voltage of 3 V when subjected to a 2.5 N load at 45 Hz. This performance surpassed that of both ZnS/PVDF-HFP (~2 V) and PANI/PVDF-HFP (~1 V) composites. The improvement was attributed to the positive charges on the surface of ZnS@PANI microspheres, which induced the alignment of polymer chains, increasing the β-phase of PVDF-HFP. Additionally, a p-n heterojunction formed at the interface of p-type PANI and n-type ZnS suppressed the internal screening effect that could reduce piezoelectric output.

A core@double-shell structure was employed by coating BTO nanowires with hyperbranched aromatic polyamide (HBP) and subsequently with PMMA using γ-APS as a coupling agent and BIBB as an initiator precursor (**Figure 5d**) [66]. The enhanced dielectric properties of BTO@HBP@PMMA nanowires were attributed to the inner HBP layer, which improved the polarization degree of the nanowires under a high electric field during the electrospinning process [67]. The outer PMMA layer prevented nanowire agglomeration, enhancing the interaction between the nanowires and PVDF, which promoted nanofiller dispersibility and improved stress-transfer efficiency. Electrospun BTO@HBP@PMMA/PVDF nanofiber-based PENGs achieved a piezoelectric output voltage of 3.4 V and a current of 0.32 μA, respectively, under a 40 N load at 10 Hz, surpassing the values obtained with the BTO/PVDF nanofiber-based PENG (~2.5 V, ~0.15 μA). The effect of polymer coating on the piezoelectric nanocomposites is illustrated in **Figure 6**, and their performance is summarized in **Table 1**.

In overall, polymer coating is highly likely to improve the interfacial interaction between nanofillers and the polymer matrix in addition to enhancing the stress-transfer effectiveness. Although only three studies reported $d_{33}$ values before and after nanofiller modifications (**Table 1**), the minimal changes in $d_{33}$ values ($\leq$5%) indicate a negligible direct impact on the intrinsic piezoelectric properties. Instead, the coating facilitates better dispersion and stability of the nanofillers within the polymer matrix, leading to a more efficient load transfer and significant improvements in output voltage and current, as demonstrated in various studies [46, 49–51, 62, 63, 66]. Among polymer materials, PDA has been used most frequently due to its simple and easy processing. Other polymer coating procedures require additional steps, such as silane and BIBB functionalization, which often involve complex conditions, including moisture-free or oxygen-free environments (**Figure 4**). Overall, the polymer coating of the nanofiller has proven to be a highly effective strategy for optimizing the functional properties of piezoelectric nanocomposites.

### 2.3. Coating of nanofillers with carbon materials

Carbon materials, including carbon black, graphene/carbon fibers, graphene oxide (GO), reduced graphene oxide (rGO), and multiwalled carbon nanotubes (MWCNTs), have been widely used as nanofillers to improve the piezoelectricity and mechanical strength of PVDF-based PENGs [36, 68–70]. Their primary role is to facilitate the formation of the highly polarized β-phase in PVDF. This effect is achieved through the interfacial interaction between the negatively charged carbon materials and the locally positively polarized -$CH_2$ groups of the PVDF chains. Additionally, these carbon materials provide pathways and carriers for charge transfer and accumulation, aiding in the alignment of dipoles in nanofillers when subjected to a high electric field applied during the electrospinning or poling process. Consequently, the electric domains within the nanofillers align with the polarization field direction, thereby enhancing their piezoelectric activity. Furthermore, the low surface energy of the carbon shell enhances nanoparticle dispersion, thereby preserving the flexibility and mechanical properties [69, 71].

BTO@C nanoparticles were synthesized through the calcination of BTO@PDA nanoparticles at 550 °C under an argon (Ar) atmosphere (**Figure 7a**) [72]. BTO@C/PVDF-TrFE composite films were then fabricated using the solution casting and poling processes. The addition of a carbon layer improved the piezoelectric performance of the BTO@C/PVDF-TrFE composite films, giving rise to a maximum output voltage of 17 V at a bending angle of 60°. This performance represented a three-fold increase compared to that of pristine BTO/PVDF-TrFE films. Furthermore, the same coating method to three different nanomaterials: BTO, PZT, and potassium sodium niobate ($KNaNbO_3$, KNN) [73]. An investigation of the effect of carbon layer thickness on the piezoelectricity of PENGs prepared with polydimethylsiloxane (PDMS) as a polymer matrix indicated that the output voltage of PENGs poled under the same conditions increased with the thickness of the carbon layer, up to 15 nm. It was believed that the carbon layer enhanced the alignment of dipoles in the nanoparticles under an external electric field. With a carbon layer thickness of 15 nm, the piezoelectric output voltage and current under a 10 N load at 10 Hz for BTO@C/PDMS (31 V and 1.8 μA), PZT@C/PDMS (37 V and 1.9 μA), and KNN@C/PDMS (14 V and 0.8 μA) PENGs consistently exceeded those of unmodified BTO/PDMS (8 V and 0.45 μA), PZT/PDMS (10 V and 0.5 μA), and KNN/PDMS (5 V and 0.35 μA) PENGs.

BTO@C nanoparticles were also used to fabricate BTO@C/PVDF composite scaffolds using a selective laser sintering (SLS) technique under an atmosphere of nitrogen [74]. The incorporation of BTO@C nanoparticles improved the mechanical properties of the composite scaffolds. Specifically, the tensile strength increased by 22.6% to 38 MPa, the tensile modulus by 18.7% to 919 MPa, the compressive strength by 71.4% to 10.8 MPa, and the compressive modulus by 40.8% to 41.4 MPa. Additionally, the carbon layer coating positively impacted the maximum output voltage and current of the PENGs, increasing them from 4.5 V to 5.7 V and from 0.06 μA to 0.08 μA, respectively.

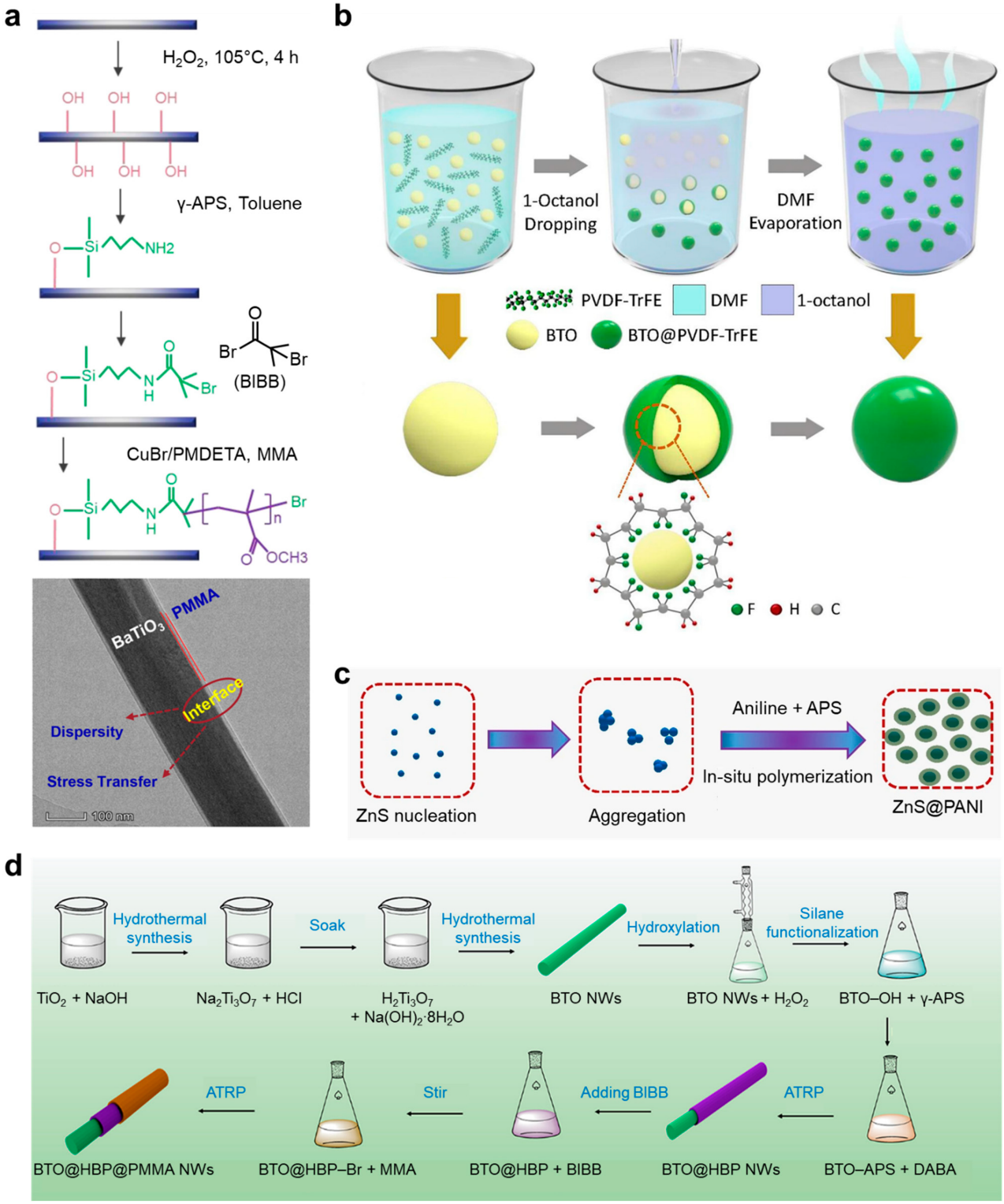


**Figure 5** • Synthesis of inorganic nanofillers coated with various polymer materials. (**a**) BTO@PMMA nanowires. Reproduced with permission from [63]. Copyright 2020, Elsevier. (**b**) BTO@PVDF-TrFE nanoparticles. Reproduced with permission from [62]. Copyright 2021, Elsevier. (**c**) ZnS@PANI microspheres [64]. (**d**) BTO@HBP@PMMA nanowires. Reproduced with permission from [66]. Copyright 2022, American Chemical Society.

A carbon layer was applied to zinc oxide (ZnO) nanoparticles, which were then used to fabricate ZnO@C/PVDF nanofiber membranes via electrospinning [75]. The ZnO@C nanoparticles not only increased the β-phase content in PVDF, but also negatively shifted the surface potential of the membrane from −130 mV to −740 mV, making this composite a promising candidate for triboelectric nanogenerators (TENGs). Additionally, the carbon outer layer of nanofillers improved the piezoelectric performance, as indicated by an increase in the $d_{33}$ values from 35.6 pC/N for the ZnO/PVDF PENG to 39.5 pC/N for the ZnO@C/PVDF PENG. The device achieved an output voltage of up to 37 V under a 14.7 N load, with a sensitivity of 0.98 V/kPa, equivalent to 3 V/N based on the effective working area of 3.3 $cm^2$.

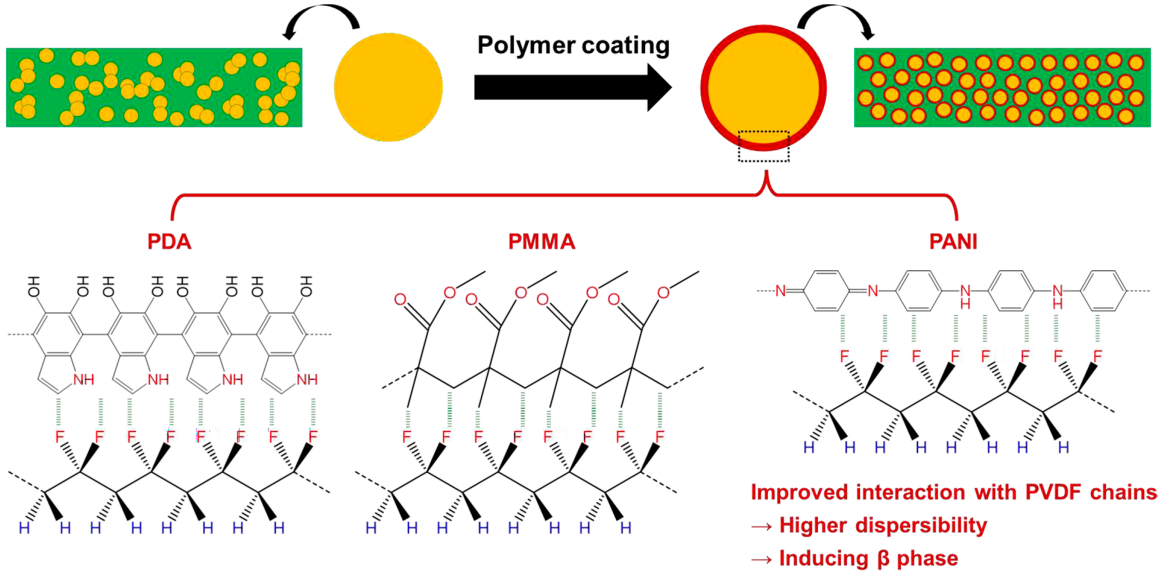


**Figure 6** • The effect of various polymer coating on inorganic nanofillers: Improved dispersibility and enhanced interfacial interaction with the polymer matrix, particularly in the case of PVDF.

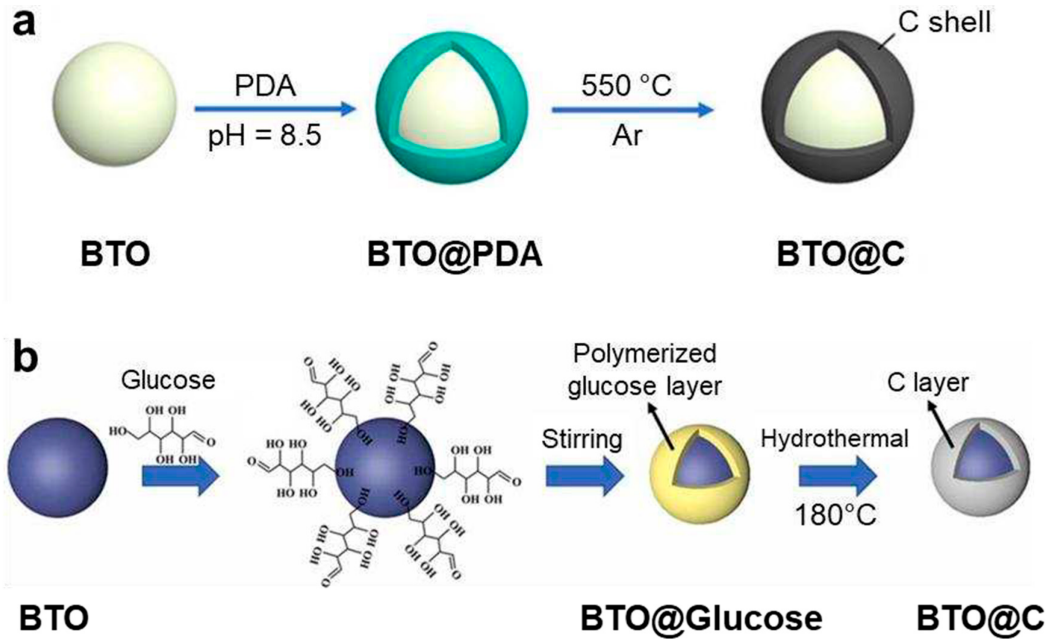


**Figure 7** • Two methods for preparing BTO@C nanoparticles: (**a**) Calcination of BTO@PDA nanoparticles. Reproduced with permission from [72]. Copyright 2019, American Chemical Society. (**b**) Glucose-assisted hydrothermal method. Reproduced with permission from [71]. Copyright 2023, Elsevier.

BTO@C particles were also synthesized using a glucose-assisted hydrothermal method, in which a carbon shell was formed through the carbonization of glucose attached to the BTO surface during the hydrothermal process (**Figure 7b**) [71]. The resulting BTO@C/PVDF-TrFE PENGs demonstrated nearly double the performance (61 V, 1.33 μA) under a bending displacement of 5 mm compared to BTO/PVDF-TrFE PENGs (37 V, 0.75 μA) under identical testing conditions. The effects of carbon coating on the nanofillers are summarized in **Figure 8**.

Carbon coating on nanofillers offers several benefits, including improved dispersibility, induction of more β-phase PVDF, and alignment of dipoles within nanofillers under a high electric field (**Figure 8**). The latter benefit appears to play the most significant role in enhancing the piezoelectric performance, as demonstrated by the substantial increase in $d_{33}$ values (≥33%) reported. This increase arises because polarization induced by the highly aligned dipoles within the material improves its ability to generate an electric charge in response to mechanical stress [18–20]. Mechanically, carbon-coated nanofillers increase strength and facilitate better stress transfer between the nanofillers and the surrounding matrix, thereby improving the overall performance [74]. While the glucose-assisted hydrothermal method requires milder synthesis condition for carbon coating, the calcination of PDA offers versatility, as PDA can be coated onto various types of surfaces [76]. However, more research on carbon-coated nanofillers is needed, as relatively few studies have explored their full potential and applications.

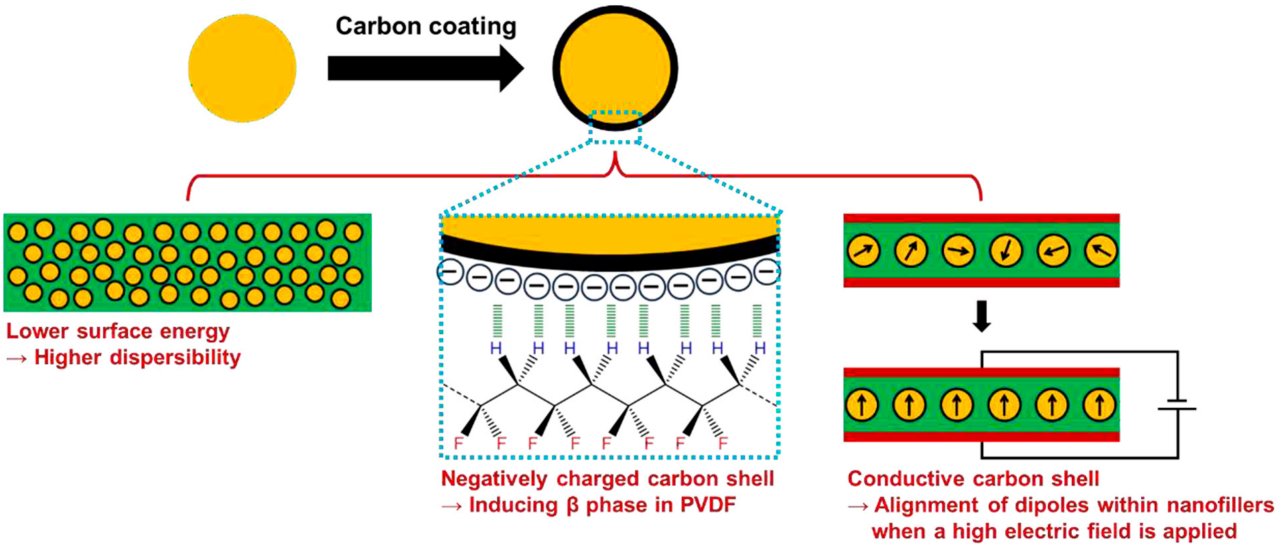


**Figure 8** • The effects of carbon coating on nanofillers.

### 2.4. Coating of nanofillers with metal oxides

Metal oxides can be used to coat piezoelectric nanofillers, with the resulting effects varying significantly depending on the specific properties of the metal oxides and the nanofillers employed, as well as the interaction between the two materials. A strontium titanate ($SrTiO_3$, STO) layer was applied to BTO nanoparticles to explore the potential coupling effect between flexoelectricity and piezoelectricity [77]. This layer was formed through the simultaneous interdiffusion of $Ba^{2+}$ and $Sr^{2+}$ cations during the hydrothermal reaction. Unlike piezoelectricity, which is generated by uniform strains, flexoelectricity is directly proportional to the strain gradient within a structure induced by bending [78]. While this phenomenon might be subtle in bulk materials, it becomes more pronounced in nanoscale and biological systems where structures carry substantial strain gradients [79]. In BTO@STO nanoparticles, the mismatched lattice parameters between $Ba^{2+}$ and $Sr^{2+}$ cations induced a strain gradient, leading to a highly polarized structure that enabled the coexistence of both piezoelectric and flexoelectric effects (**Figure 9**). To support these experimental findings, density functional theory (DFT) and finite element method (FEM) calculations were conducted. With an STO shell thickness of 33.5 nm, the BTO@STO/PDMS nanocomposite exhibited an output voltage (~160 V) and current (~0.7 μA) that were more than double those of a composite based solely on pure BTO nanoparticles.

In an attempt to synergize the effects of magnetic iron (II,III) oxide ($Fe_3O_4$) and dielectric manganese dioxide ($MnO_2$), porous $Fe_3O_4$@$MnO_2$ nanoparticles were synthesized as multifunctional magnetic–dielectric nanofillers for use in both piezoelectric and electromagnetic (EM) shielding devices [80]. Upon incorporation into PVDF nanofiber mats via the electrospinning process, the $Fe_3O_4$@$MnO_2$ nanoparticles achieved a maximum output voltage of 26.3 V under a 90 N force at 3 Hz, exhibiting a sensitivity of 0.3 V/N in the 50 N to 90 N range. The observed increase in piezoelectricity was attributed to the rise in the β-phase content in PVDF, induced by the negative surface charge of $Fe_3O_4$@$MnO_2$ nanoparticles. The unique combination of a magnetic core ($Fe_3O_4$) and a dielectric shell ($MnO_2$) in the particles led to both magnetic and dielectric losses. These losses are crucial for the dissipation of electromagnetic energy [81], making the composite well-suited for EM shielding applications. Reflection loss (RL) measurements conducted at 8–12 GHz (X-band) demonstrated that the maximum RL value was directly proportional to the nanoparticle content in the composites.

Various approaches have been undertaken to enhance the piezoelectric performance of PENGs based on gallium nitride (GaN) materials [82, 83]. One innovative solution involved epitaxially growing GaN nanowires coated with vanadium pentoxide ($V_2O_5$) [84]. This coating aimed to establish a potential barrier at the interface between n-GaN and p-$V_2O_5$, thereby suppressing carrier transport across the p-n heterojunction. As a consequence, the GaN@$V_2O_5$/PDMS PENG (27 V and 0.085 μA) significantly outperformed the GaN/PDMS PENG (9 V and 0.032 μA) in piezoelectric output values. Furthermore, by replacing the outer shell material with $Al_2O_3$, their device reached a maximum output voltage of up to 30 V and a current of 0.12 μA (**Figure 10**) [85].

There are few studies reporting the use of metal oxide coating on nanofillers for enhanced piezoelectricity, which presents both a challenge and an opportunity. The flexoelectric effect, demonstrated through the generation of electric polarization in response to a strain gradient, is particularly promising because it is not limited by material symmetry or Curie temperature, broadening its applicability [77]. It is especially advantageous in nanoscale systems, where large strain gradients occur naturally, making it highly relevant for sensing and energy-harvesting applications [86]. Lattice-mismatched heterostructures can potentially be applied to other perovskites or metal oxides. Therefore, selecting and optimizing suitable materials for flexoelectricity will be critical to unlocking its full potential and transitioning from theoretical studies to practical applications.

The concept of GaN@metal oxide-based PENGs is intriguing, as these materials give relatively high voltages when subjected to mechanical stimuli such as finger tapping or bending. While these devices show promise, the fabrication methods, including epitaxial growth and atomic layer deposition, require sophisticated equipment. This shortcoming presents a challenge for developing more accessible and straightforward techniques but also underscores the potential for future advancements in this area.

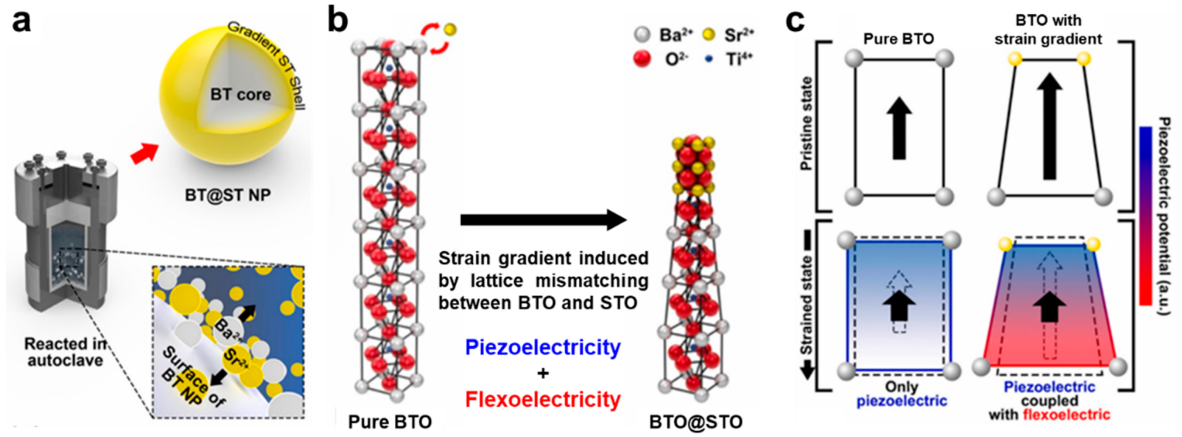


**Figure 9** • BTO@STO nanoparticles. (**a**) Formation of the gradient STO shell on the surface of pure BTO nanoparticles during the hydrothermal reaction. (**b**) Enhanced piezoelectricity due to the strain gradient induced by the STO shell. (**c**) Comparison of piezoelectric potential generated in pure BTO and BTO@STO nanoparticles under pristine and stressed states. Reproduced with permission from [77]. Copyright 2021, Elsevier.

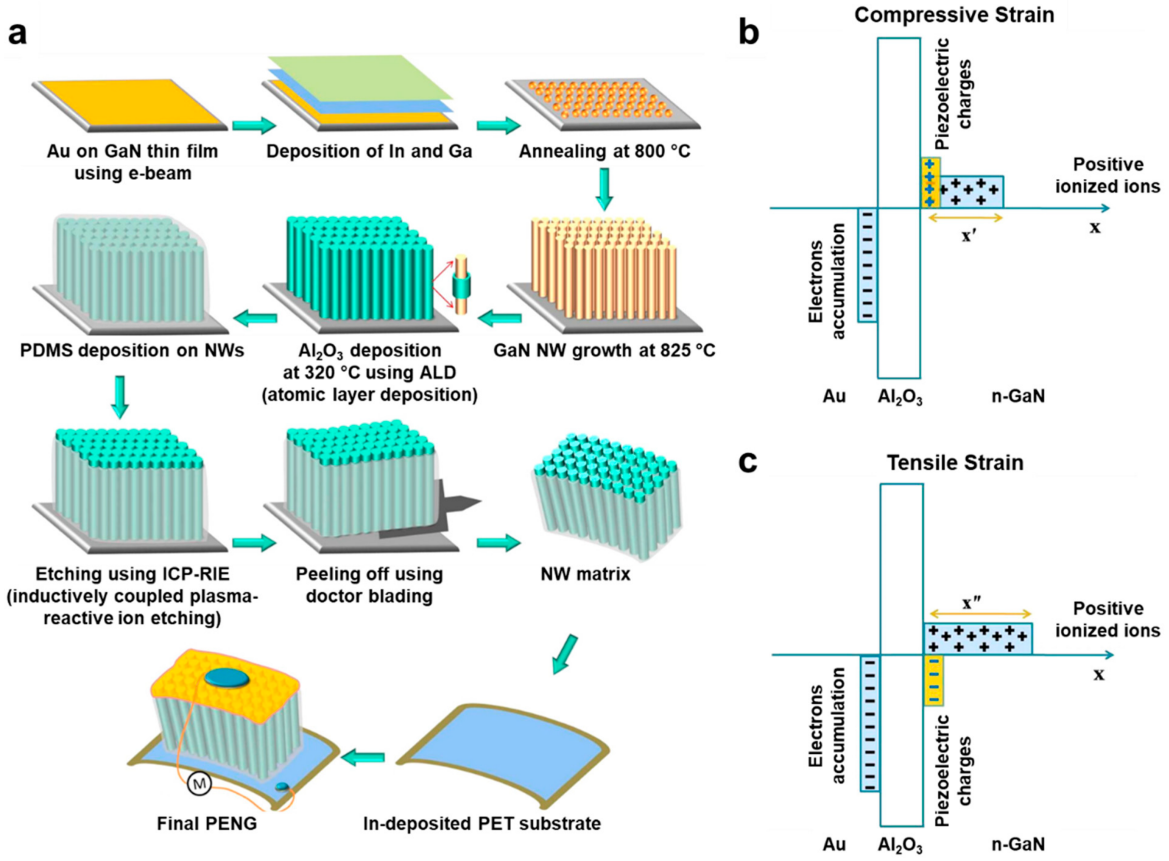


**Figure 10** • GaN@Al2$O_3$/PDMS PENG. (**a**) Fabrication of the GaN@Al2$O_3$/PDMS PENG device. (**b**) Piezoelectric charges generated under compressive strain. (**c**) Piezoelectric charges generated under tensile strain. Reproduced with permission from [85]. Copyright 2020, Elsevier.

## 3. Decorating nanofillers with smaller nanoparticles

In some cases, nanofillers are decorated with smaller nanoparticles on their surfaces, yet they are still referred to as "core@shell" structures. While coating involves forming a continuous and uniform layer over the entire surface of a nanoparticle, decorating involves attaching smaller nanoparticles or clusters of atoms to the surface of a larger nanoparticle, giving rise to partial coverage. Decorated nanofillers can create synergistic effects by combining the properties of the core and the decorating particles.

Small Ag nanoparticles were grafted onto the surface of ZnO, which were then used to produce electrospun Ag-decorated ZnO/PVDF nanofiber PENGs [87]. The Ag nanoparticles improved the conductivity and dielectric properties of the nanofillers, enhancing the stretching polarization of the solution during the electrospinning and curing processes and thereby promoting the formation of β-PVDF (**Figure 11a**). Compared to

pristine ZnO/PVDF PENGs, the output voltage and current under a 50 N load at 5 Hz increased from 11.1 V and 0.634 μA to 15.0 V and 1.775 μA, respectively. The conductive Ag nanoparticles facilitated β-phase formation in PVDF and dipole alignment during the electrospinning process. The Ag-decorated ZnO/PVDF PENGs exhibited a peak sensitivity of 2.4 V/kPa (~0.48 V/N, based on an effective area of 2 $cm^2$), within the range of 6.4 N to 12.8 N. Similarly, BCZT nanowires were decorated with Ag nanoparticles for the same purpose (enhanced conductivity and dielectric constant) [88]. The Ag-decorated BCZT/PVDF-TrFE composite, prepared with 0.04 M $AgNO_3$ solution, improved the $d_{33}$ value (from 21 to 28 pC/N) and output voltage (from 1.5 to 3.5 V) compared to the pure BCZT/PVDF-TrFE composite.

The dispersibility of MWCNTs in PVDF was enhanced by decorating them with silicon dioxide ($SiO_2$) nanoparticles [89]. While the negatively charged MWCNTs increased the β-phase content in PVDF, hydrophilic $SiO_2$ not only improved the dispersion of the nanofillers, but also increased the dielectric loss and reflected EM waves, making the composite suitable for EM shielding applications (**Figure 11b**). The $SiO_2$-decorated MWCNT/PVDF composites exhibited an output voltage and current of 45 V and 4.8 μA, respectively, under a 0.4 MPa (~80 N, given the effective area of the composite) load at 4 Hz. Additionally, these composites effectively blocked 99% of the incident EM radiation in the X-band region (8.2–12.4 GHz), with absorption and reflection losses of 86% and 14%, respectively. Similar attempts have been made using ZnO-decorated carbon materials to improve the dispersion of nanofillers in PVDF composites, such as ZnO-decorated SWCNT/PVDF [90] and ZnO-decorated rGO/PVDF [91]. A systematic study was conducted to determine the optimal fractions of ZnO (10 wt%) and rGO (1.5 wt%) in PVDF, and ZnO-decorated rGO using these proportions [91]. Interestingly, the composite prepared with hydrothermally synthesized ZnO-decorated rGO (153 V) showed superior performance compared to the composite prepared by directly mixing ZnO and rGO (60.95 V) under a 50 N load at 15 Hz, owing to the organized arrangement of ZnO on the surface of rGO, which facilitates the formation of highly ordered β-phase PVDF chains. Additionally, Cu-Ni-nanoalloy-decorated CNTs using the electroless technique [92], a chemical deposition method that enables uniform metal coating without the use of external electrical current. Due to the improved dispersion of the Cu-Ni-decorated CNTs in polar DMF, the resulting composite film achieved an output voltage of 35 V under a 98 N load at 8 Hz along with a power density of 204 $\mu W/cm^3$.

The radial piezoelectricity of boron nitride nanotubes (BNNTs) was enhanced by chemically incorporating ZnO quantum dots onto their surfaces [93]. PFM measurements confirmed this improvement, revealing larger piezoelectric coefficients for ZnO-decorated BNNTs (0.340 pC/N) than those for undecorated BNNTs (0.238 pC/N). As expected, the piezoelectric performance of the ZnO-decorated BNNT/PDMS PENG (18.56 V and 382.2 nA) generated by bending surpassed that of the BNNT/PDMS PENG (12.74 V and 238.5 nA). After poling, the device's performance peaked at 30.59 V and 734.5 nA.

Inspired by the features of strawberries, the surface of BTO@PDA nanoparticles was decorated with smaller Ag nanoparticles through an in situ growth process to exploit the combined effects of PDA and Ag (**Figure 11d**) [94]. The resulting strawberry-like Ag-decorated BTO@PDA nanoparticles and PVDF powders were separately dispersed in ethanol. These were then mixed by sonication and stirring to produce composite powders, which were used to create polymer scaffolds using the SLS technique. This strawberry-like structure was designed to synergistically combine the dual effects of polymeric (PDA) and the conductive (Ag) outer layers. The PDA served to improve the dispersibility and stress-transfer efficiency of the nanoparticles in the polymeric matrix, as in previous cases. Simultaneously, the conductive Ag nanoparticles enhanced the strength of the electric field applied on the BTO particles during the SLS process, promoting better dipole alignment in the structure. Additionally, the antibacterial properties of the Ag nanoparticles were expected to enhance the antibacterial activities of the composites. As a consequence of the Ag decoration of the nanofillers, the output voltage and current of the composites increased from 7.4 V and 0.09 μA to 10 V and 0.14 μA, respectively. Furthermore, the composites exhibited an 80% inhibition rate against *Escherichia coli*, determined by comparing the optical density of bacterial suspensions with and without the composites.

Decorating nanofillers offers several advantages for enhancing piezoelectricity. The partial coverage of nanofillers with smaller nanoparticles can improve dispersion and stability within a polymer matrix, ensuring uniform distribution and preventing aggregation. Additionally, the incorporation of conductive nanoparticles through decoration can enhance the overall electrical conductivity of the composite, facilitating more efficient charge transfer and improving the piezoelectric output. However, a uniform and continuous coating may be more advantageous for achieving consistent dipole alignment and effective stress transfer throughout the material. As shown in **Table 1**, **Table 2**, **Table 3** and **Table 4**, nanocomposites with decorated nanofillers typically require higher forces to reach their maximum output performance compared to those with coated nanofillers. Nevertheless, decorated nanoparticles remain highly effective in catalytic applications. The partial coverage provided by decoration increases surface roughness and active surface area, both of which are crucial for enhancing catalytic activity. Furthermore, synergistic effects between the core and decorating particles can significantly boost catalytic performance. For instance, metal-decorated BTO heterostructures, which combine the localized surface plasmon resonance (LSPR) of metal nanoparticles with the piezoelectricity of BTO, have been extensively studied for enhancing photocatalytic efficiency. The enhanced efficiency is achieved by leveraging the built-in piezoelectric field to suppress electron–hole recombination [95–97].

The piezoelectric nanocomposites based on nanofillers coated or decorated with carbon materials, metal oxides, and various nanoparticles are summarized in **Table 2**, **Table 3** and **Table 4**.

## 4. Doping nanofillers

Chemical doping is a feasible method for enhancing the piezoelectricity of nanofillers through ion substitution in their crystal structure by dopants. Depending on the ionic radius and valence of dopants, the ion substitution induces lattice strain and distortion that can affect the crystal structure, dielectric properties, and surface polarization of nanofillers, thereby enhancing their piezoelectricity (**Figure 12a**) [98, 99]. Given this perspective, the output performance of PENGs can be enhanced through the careful selection of doping elements for nanofillers [100].

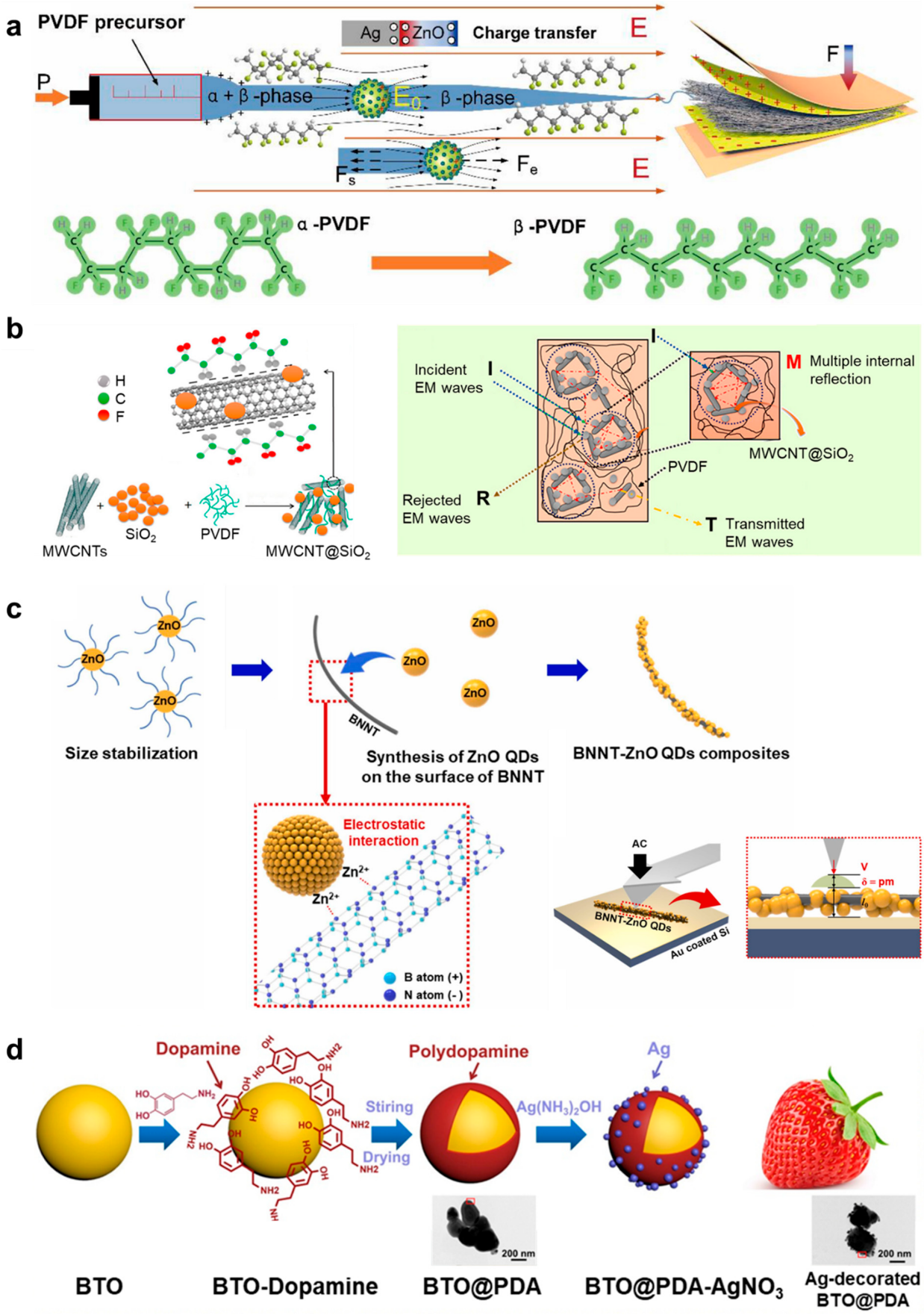


**Figure 11** • Decorated-nanofillers. (**a**) Ag-decorated ZnO nanofillers. Reproduced with permission from [87]. Copyright 2022, Elsevier. (**b**) $SiO_2$-decorated MWCNT nanofillers. Reproduced with permission from [89]. Copyright 2018, American Chemical Society. (**c**) ZnO-decorated BNNT nanofillers. Reproduced with permission from [93]. Copyright 2021, Elsevier. (**d**) Ag-decorated BTO@PDA nanofillers. Reproduced with permission from [94]. Copyright 2020, Elsevier.

**Table 1 •** Summary of piezoelectric nanocomposites based on nanofillers coated with polymers. The percentage values in parentheses indicate the increase in performance compared to nanocomposites with unmodified nanofillers.

| Ref. | Nanofiller parameters | | | | Nanofiller fraction | Polymer material | Fabrication method | Testing method | Nanocomposite performance parameters | | | | |
|---|---|---|---|---|---|---|---|---|---|---|---|---|---|
| | Material (Core@Shell) | Shape | Diameter (Shell thickness) | $d_{33}$ (pC/N) | | | | | Voltage (V) | Current (μA) | $d_{33}$ (pC/N) | Power density (load) | Sensitivity (range) |
| [49] | BTO@PDA | Sphere | ~114 nm (~14.5 nm) | - | 17 wt% | PVDF | Solution casting, Poling | Pressing (12 N at 1 Hz) | 9.3 (98% ↑) | 0.086 (60% ↑) | - | 0.122 μW/cm² (70 MΩ) (100% ↑) | ~0.06 V/N (12–243 N) |
| [50] | BTO@PDA | Sphere | ~115 nm (~20 nm) | - | 5 wt% | PVDF | Electrospinning | Pressing (3 N at 1 Hz) | 13.5 (78% ↑) | 0.5 (40% ↑) | 22.56 (~4% ↑) | - | 3.95 V/N (0.07–3 N) (75% ↑) |
| [46] | BTO@PDA | Sphere | ~115 nm (~20 nm) | - | 3 wt% | PVDF | Electrospinning | Pressing (3 N at 1 Hz) | ~8.3 (130% ↑) | ~0.4 (300% ↑) | 35.8 (~2% ↑) | - | −0.38 V/N (0.22–19.33 N) |
| [51] | BTO@PDA | Sphere | ~120 nm (~15 nm) | - | 20 wt% | PVDF-TrFE | Electrospinning Sonication | Pressing (700 N at 3 Hz) | 6 (380% ↑) | 1.5 (150% ↑) | - | 0.88 μW/cm² (5 MΩ) | - |
| [52] | BTO@PDA | Sphere | ~120 nm (~20 nm) | - | 5 wt% | Cellulose /PVDF-g-MA | Electrospinning Sonication | Pressing (5 N at 3 Hz) | 3.2 | 0.25 | 27.2 | 1.72 μW/cm² (10 MΩ) | - |
| [54] | BTO@PDA | Rod | ~254 nm (~20 nm) | 41 (5% ↑) | 7 wt% | PVDF-TrFE | Electrospinning Poling | Pressing (5 N at 1 Hz) | 18.2 | 1.5 | 34 | 3.18 μW/cm² (50 MΩ) | 4.3 V/N (< 1.5 N) |
| [54] | BCZT@PDA | Sphere | ~650 nm (~20 nm) | - | 20 vol% | PLA | Solution casting | Finger tapping (~2 N) | 14.4 | 0.55 | - | 12.8 μW/cm² (3.5 MΩ) | - |
| [55] | HZTO@PDA | Rod | ~320 nm (~17 nm) | 26 | 20 vol% | PLA | Solution casting | Finger tapping (~2 N) | 5.41 | 0.26 | - | 1.85 μW/cm² (2.5 MΩ) | - |
| [62] | BTO@PVDF-TrFE | Sphere | ~70.4 nm (~5 nm) | - | 23 wt% | PVDF-TrFE | Doctor blade coating, Poling | Pressing (100 N at 2.5 Hz) | 59.5 (380% ↑) | 6.52 (100% ↑) | 20 | 18.42 μW/cm² (10 MΩ) | - |
| [63] | BTO@PMMA | Rod | ~180 nm (~10 nm) | 20 | 10 wt% | PVDF-TrFE | Electrospinning | Bending (4 mm at 2 Hz) | 12.6 (58% ↑) | 1.3 (44% ↑) | - | 0.68 μW/cm² (7.2 MΩ) (120% ↑) | - |
| [64] | ZnS@PANI | Sphere | ~3.5 μm (~400 nm) | - | 2 wt% | PVDF-HFP | Electrospinning | Pressing (2.5 N at 45 Hz) | 3 | - | - | 2.92 μW/cm² | - |
| [66] | BTO@HBP @PMMA | Rod | ~340 nm (HBP: ~20 nm) (PMMA: ~13 nm) | - | 7 wt% | PVDF | Electrospinning | Pressing (40 N at 10 Hz) | 3.4 (36% ↑) | 0.32 (113% ↑) | - | 0.58 μW/cm² (10 MΩ) | - |

**Table 2 •** Summary of piezoelectric nanocomposites based on nanofillers coated with carbon materials. The percentage values in parentheses indicate the increase in performance compared to nanocomposites with unmodified nanofillers.

| Ref. | Nanofiller | | | | | | | | Nanocomposite performance parameters | | | | |
|---|---|---|---|---|---|---|---|---|---|---|---|---|---|
| | Material (Core@Shell) | Shape | Diameter (Shell thickness) | $d_{33}$ (pC/N) | Nanofiller fraction | Polymer material | Fabrication method | Testing method | Voltage (V) | Current (μA) | $d_{33}$ (pC/N) | Power density (load) | Sensitivity (range) |
| [72] | BTO@C | Sphere | ~120 nm (10–15 nm) | - | 15 wt% | PVDF-TrFE | Solution casting, Poling | Bending (1.5 cm at 1.5 Hz) | 17 (200% ↑) | - | ~27 | 2.38 μW/cm² (13.2 MΩ) | - |
| [73] | BTO@C | Sphere | ~150 nm (15 nm) | - | 15 wt% | PDMS | Solution casting, Poling | Pressing (10 N at 10 Hz) | 31 (250% ↑) | 1.8 (320% ↑) | ~40 (100% ↑) | 45.4 μW/cm² (1900% ↑) | - |
| [74] | BTO@C | Sphere | 213 nm (~3.5 nm) | - | 1 wt% | PVDF | SLS | Pressing | 5.7 (27% ↑) | 0.08 (33% ↑) | - | - | - |
| [71] | BTO@C | Sphere | ~200 nm (~2 nm) | - | 15 wt% | PVDF-TrFE | Solution casting, Poling | Bending (5 mm at 1 Hz) | 61 (65% ↑) | 1.33 (77% ↑) | 32 (33% ↑) | 3.47 μW/cm² (70 MΩ) (140% ↑) | - |
| [73] | KNN@C | Sphere | ~150 nm (15 nm) | - | 15 wt% | PDMS | Solution casting, Poling | Pressing (10 N at 10 Hz) | 14 (160% ↑) | 0.8 (129% ↑) | - | 9.9 μW/cm² (1140% ↑) | - |
| [75] | ZnO@C | Sphere | ~200 nm (10–15 nm) | - | 5 wt% | PVDF | Electrospinning | Pressing (14.7 N) | 37 | - | 39.5 | - | 0.98 V/kPa ~3 V/N (≤ 14.7 N) |

**Table 3 •** Summary of piezoelectric nanocomposites based on nanofillers coated with metal oxides. The percentage values in parentheses indicate the increase in performance compared to nanocomposites with unmodified nanofillers.

| Ref. | Nanofiller | | | | | | | | Nanocomposite performance parameters | | | | |
|---|---|---|---|---|---|---|---|---|---|---|---|---|---|
| | Material (Core@Shell) | Shape | Diameter (Shell thickness) | $d_{33}$ (pC/N) | Nanofiller fraction | Polymer material | Fabrication method | Testing method | Voltage (V) | Current (μA) | $d_{33}$ (pC/N) | Power density (load) | Sensitivity (range) |
| [77] | BTO@STO | Sphere | 400 nm (33.5 nm) | 49.6 (99% ↑) | 20 wt% | PDMS | Spin casting | Bending | ~160 (220% ↑) | ~0.7 (250% ↑) | 118 (129% ↑) | - | - |
| [80] | $Fe_3O_4$@$MnO_2$ | Sphere | ~1300 nm (40 nm) | - | 4 wt% | PVDF | Electrospinning | Pressing (90 N at 3 Hz) | 26.3 | - | - | - | ~0.3 V/N (50–90 N) |
| [84] | GaN@$V_2O_5$ | Sphere | 78 nm (17 nm) | - | - | PDMS | Epitaxial growth, ALD, Solution casting | Bending (12 Hz) | 27 (200% ↑) | 0.085 (166% ↑) | - | - | - |
| [85] | GaN@$Al_2O_3$ | Sphere | 52 nm (6 nm) | - | - | PDMS | Epitaxial growth, ALD, Solution casting | Finger tapping (3 Hz) | 30 | 0.1 | - | 0.4 μW/cm² (~100 MΩ) | - |

**Table 4 •** Summary of piezoelectric nanocomposites based on nanofillers decorated with smaller nanoparticles. The percentage values in parentheses indicate the increase in performance compared to nanocomposites with unmodified nanofillers.

| Ref. | Nanofiller | | | | | | | | Nanocomposite performance parameters | | | | |
|---|---|---|---|---|---|---|---|---|---|---|---|---|---|
| | Material (Core@Shell) | Shape | Diameter (Shell thickness) | $d_{33}$ (pC/N) | Nanofiller fraction | Polymer material | Fabrication method | Testing method | Voltage (V) | Current (μA) | $d_{33}$ (pC/N) | Power density (load) | Sensitivity (range) |
| [87] | Ag-decorated ZnO | Sphere Sphere | Ag: 120 nm ZnO: 1–3 μm | - | 5 wt% | PVDF | Electrospinning | Pressing (50 N at 5 Hz) | 15 (35% ↑) | 1.775 (180% ↑) | - | - | 2.4 V/kPa ~0.48 V/N (6.4–12.8 N) |
| [88] | Ag-decorated ZnO | Sphere Rod | Ag: 70–130 nm BCZT: ~300 nm | - | 3 wt% | PVDF-TrFE | Tape casting | Pressing (~50N at 2 Hz) | 3.5 (130% ↑) | 1.8 | ~28 (33% ↑) | 0.45 μW/cm² (4 MΩ) | 0.016 V/kPa ~0.05 V/N (10–50 N) |
| [89] | $SiO_2$-decorated MWCNT | Sphere Wire | $SiO_2$: ~25 nm MWCNT: ~5 nm | - | 1 wt% | PVDF | Solution casting | Pressing (~80 N at 4 Hz) | 45 | 4.8 | 53 | ~54 μW/cm² (~100 MΩ) | - |
| [90] | ZnO-decorated SWCNT | Sphere Wire | ZnO: 200 nm SWCNT: - | - | 0.75 wt% | PVDF | Electrospinning | Finger tapping (6Hz) | 3.9 | 0.453 | - | 8.1 μW/cm² (10 MΩ) | - |
| [91] | ZnO-decorated rGO | Rod Sheet | ZnO: 20 nm rGO: - | - | 10 wt% (ZnO) 1.5 wt% (rGO) | PVDF | Doctor blade coating | Pressing (50N at 15 Hz) | 153 (665% ↑) | 2.5 μA/cm² | 33 | 28.38 μW/cm² (6 MΩ) | - |
| [92] | Cu-Ni-alloy-decorated CNT | Sphere Wire | Cu-Ni alloy: 10–80 nm CNT: 50–200 nm | - | 1 μL of Cu-Ni-CNT dispersion in 1g of PVDF | PVDF | Spin-coating | Pressing (98 N at 8 Hz) | 35 | 0.3 μA/cm² | 160 | 204 μW/cm² (2 MΩ) | ~2.7 V/kgf ~0.28 V/N (14.7–98 N) |
| [93] | ZnO-decorated BNNT | Sphere Wire | ZnO: ~20 nm BNNT: ~10 nm | 0.34 (43% ↑) | 0.18 wt% | PDMS | Solution casting | Bending (16–30 Hz) | 18.56 (45% ↑) | 0.38 (60% ↑) | −60.3 (42% ↑) | - | - |
| [94] | Ag-decorated BTO@PDA | Sphere Sphere | Ag: 24.5 nm BTO: ~ 500 nm (PDA thickness: 10 nm) | - | ~3.3 wt% | PVDF | SLS | Pressing | 10 (35% ↑) | 0.14 (55% ↑) | 8.2 (50% ↑) | 1.7 μW/cm² | - |

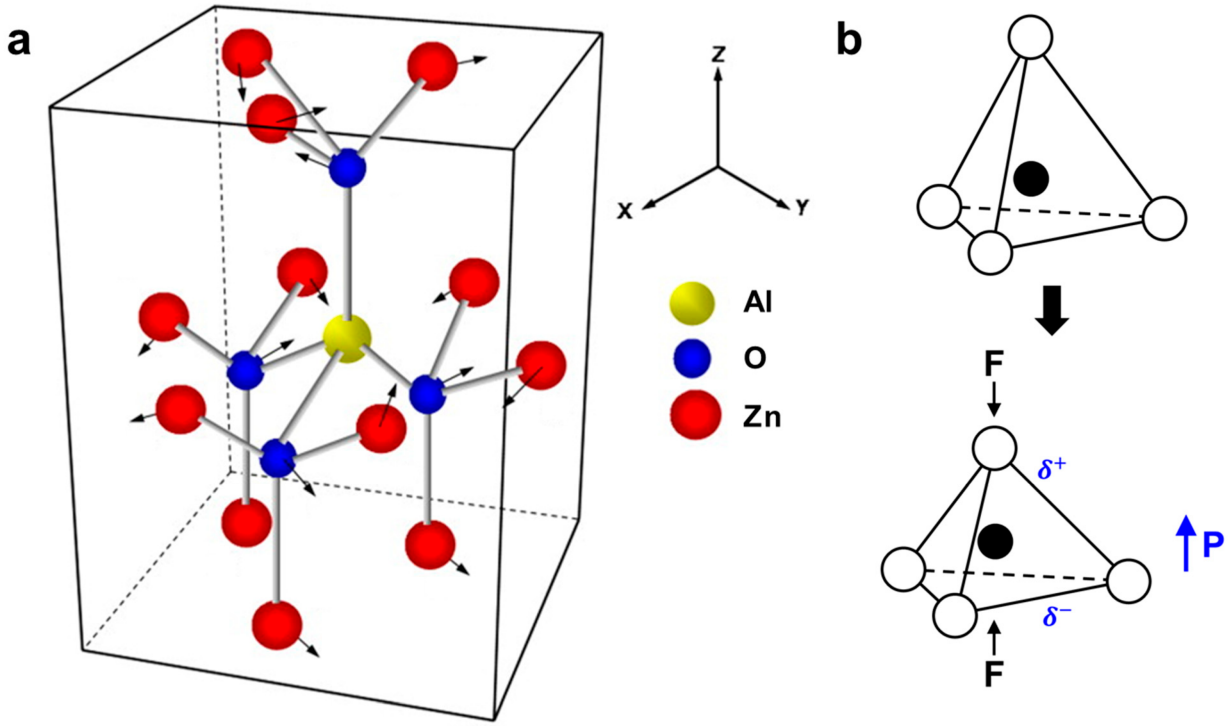


**Figure 12** • Effect of doping in ZnO crystals and their piezoelectricity. (**a**) Schematic diagram illustrating the vicinity of an Al impurity within the ZnO crystal. The arrows indicate the direction of absolute atomic movements caused by defect-induced perturbation. Reproduced with permission from [99]. Copyright 2010, Elsevier. (**b**) $Zn^{2+}$ cations (black) and $O^{2-}$ anions (white) are tetrahedrally coordinated (top). Polarization (P) induced by an applied force (F) results in a dipole moment (bottom).

### 4.1. Doped ZnO-based nanofillers

Zinc oxide (ZnO) is one of the most extensively studied materials that has been applied in PENGs due to its notable piezoelectric properties. The piezoelectric effect in ZnO arises from strain-induced polarization along the c-axis in a wurtzite crystal structure where $Zn^{2+}$ cations are tetrahedrally coordinated with $O^{2-}$ anions (**Figure 12b**) [101, 102]. Doping ZnO can enhance its piezoelectricity either by reducing the free-electron concentration in ZnO to suppress the screening effect (p-type doping), or by inducing lattice strain along the c-axis in the crystal structure. The lattice strain arising from the substitution of $Zn^{2+}$ or $O^{2-}$ sites with larger ionic species generates polarization that increases the piezopotential [103]. This section introduces some recent studies in which alkaline metals, alkaline earth metals, and transition metals were used as dopants in ZnO to enhance the piezoelectric performance of the nanocomposites.

ZnO nanoparticles doped with four different cations (Co, Na, Ag, and Li) were investigated, revealing that the Li-ZnO/PVDF-TrFE PENG—fabricated via spin-coating, annealing, and poling—exhibited the highest output voltage of 3.43 V under an applied force of 0.8 N at 1 Hz. By comparison, PENGs based on pure ZnO, Co-ZnO, Na-ZnO, and Ag-ZnO nanoparticles produced output voltages of 0.38 V, 0.47 V, 1.87 V, and 2.04 V, respectively. While this study emphasized the role of dopant parameters such as ionic radius and charge state in influencing piezoelectric properties, no definitive correlations or conclusions were established [47].

A 2 wt% Co-ZnO/PVDF-HFP composite fabricated by electrospinning generated an output voltage of 2.8 V under 2.5 N at 50 Hz [104]. Similarly, a 2 wt% Fe-ZnO/PVDF PENG prepared via solution-casting method followed by γ-irradiation produced an output voltage of 2.4 V under 2.5 N at 6 Hz [105]. The effects of Co- and Fe-doping could not be compared directly as the fabrication and testing methods were different. One interesting observation was that γ-irradiation induced the formation of defects, unsaturated bonds, and free radicals in the composite material, giving rise to an increase in the output voltage from 1.1 V to 2.4 V.

Fe-ZnO/PVDF-TrFE PENGs were fabricated using a simple solution casting method, with an iron-doping ratio of 0.05, ($Zn_{0.95}Fe_{0.05}O$), yielding a maximum output voltage reached 7 V by finger tapping [106] while Ca-ZnO/PVDF-TrFE PENGs prepared similarly produced only 0.289 V under 0.5 N at 100 Hz [107]. In a separate study, La-doping of ZnO nanorods was proposed to enhance the piezoelectric performance due to the large ionic radius and excess positive charge of $La^{3+}$ ions, which can induce strong polarization and reduce charge screening effects [108]. The output performance of the resulting La-ZnO/PDMS PENG (18V, 0.1 μA under 2 N) was further improved to 23 V and 0.1 μA after oxygen annealing of La-ZnO nanorods at 600 °C prior to incorporation into PDMS. This enhancement is attributed to an increased defect density—particularly oxygen vacancies—induced during annealing, which is believed to improve the piezoelectric properties of the nanorods [109].

A hybrid piezoelectric paper was produced through the in situ synthesis of V-ZnO microflowers in bacterial cellulose (BC) [110]. The $d_{33}$ value of V-ZnO (65.5 pC/N) was more than six times that of pristine ZnO (~10 pC/N), confirming significant improvement in piezoelectricity due to V-doping. The resulting V-ZnO/BC PENG delivered a maximum output voltage and current of 1.5 V and 0.08 μA, respectively, under bending and releasing.

A substantial improvement in the $d_{33}$ value, from ~12.4 pC/N to ~420 pC/N, was achieved through the Y-doping of ZnO [111]. Y-doping is believed to alter the direction of preferential crystallization, transforming 1D ZnO nanorods into 2D Y-ZnO nanosheets. The Y-ZnO/PDMS PENG generated an output voltage of 20 V through finger tapping (~0.98 N), while the device prepared with pure ZnO nanorods generated only 2 V. The dopant's ionic charge-to-crystal radius ratio was suggested as a key factor influencing the piezoelectric response of ZnO nanocrystals.

PENGs fabricated by incorporating Nd-ZnO [112], Tb-ZnO [113], and Ba-ZnO [114] nanorods into PDMS matrices resulted in maximum output voltages of 31 V, 9 V, and 10.5 V, respectively. Notably, the Nd-ZnO nanorods, with a $d_{33}$ value of 512 pC/N, produced the highest output voltage (31 V). However, the Ba-ZnO-based PENG (10.5 V) demonstrated efficient electromechanical conversion despite a lower $d_{33}$ value of 41.28 pC/N. The piezoelectric nanocomposites based on doped ZnO nanofillers are summarized in **Table 5**.

### 4.2. Doped and co-doped perovskite-based nanofillers

A perovskite is a crystal with the general chemical formula $ABO_3$, where A-site cations occupy the corners, B-site cations are at the center, and oxygen anions are located at the faces of a cubic unit cell (**Figure 13a**). Generally, A-site cations are alkaline earth or rare earth metals, while B-site cations are transition metals. To make perovskites piezoelectric, one or more axial lengths (tetragonal or orthorhombic), axial angles (rhombohedral) or both (monoclinic), need to be modified to achieve a non-centrosymmetric crystal structure (**Figure 13c**) [115]. In this regard, doping through the substitution of A- and B-site cations is a straightforward and effective method to enhance the piezoelectric properties of perovskites [28, 30, 116].

Over the past five years, A-site-substituted BTO and bismuth ferrite ($BiFeO_3$, BFO) perovskites have been actively explored as nanofillers in piezoelectric composites. Superior piezoelectricity was confirmed for Ce-BTO (9.5 pm/V) compared to pristine BTO (7.7 pm/V), as measured by the local piezoresponse (amplitude vs. voltage) using PFM [117]. Electrospun Ce-BTO/PVDF-TrFE nanofibers generated maximum output values of 0.29 V and 0.36 μA. A Sr-BTO/PVDF composite fabricated via tape casting and annealing achieved an output voltage of 15 V under finger tapping (~10 N at 5 Hz) [118]. Related work includes Sr-BFO/PVDF [119] and Ba-BFO/PDMS [120] PENGs, in which A-site substitution enhanced polarization within the BFO crystal structure, leading to improved piezoelectric performance compared to pristine BFO. The Sr-BFO/PDMS PENG produced an output voltage of 6.53 V and a current of 0.64 μA under a 10 N load at 1 Hz, which increased to 26.17 V at 5 Hz. In comparison, the Ba-BFO/PVDF PENG delivered 20 V and 62.6 μA under finger tapping.

Several research efforts have focused on enhancing the piezoelectric properties of BFO through co-substitution at both A- and B-sites. Ba/Zr co-doping was shown to improve the dielectric, ferroelectric, and magnetic properties of BFO nanoparticles while reducing leakage current [121]. A Ba/Zr-BFO/PVDF PENG fabricated via solution casting and annealing produced an output voltage of 20 V, which increased to 30 V after electrical poling [122]. PENGs based on Sm/Ti-doped BFO nanoparticles dispersed in a silicone rubber matrix were also developed, showing an increase in output voltage and current from 3 V and 0.6 μA to 5 V and 0.9 μA, respectively, under a 35 N load at 1 Hz [123]. Additionally, Sm/Ti-doped BFO nanoparticles were distributed onto a cellulose template and processed via freeze-drying and sintering to form interconnected 3D porous structures. This architecture was designed to enhance stress transfer efficiency compared to composites with randomly dispersed nanoparticles. As a result, the piezoelectric performance of the PENGs increased to 16 V and 2.8 μA.

For other perovskite materials, Al-doped zinc stannate ($ZnSnO_3$) nanocubes were synthesized by substituting $Zn^{2+}$ cations (0.88 Å) with $Al^{3+}$ (0.62 Å), resulting in significant lattice distortion due to the ionic radius mismatch with $Sn^{4+}$ (0.83 Å) cations [124]. An Al-$ZnSnO_3$/PDMS PENG fabricated via a simple solution casting method exhibited notable piezoelectric performance, generating output values of 110 V and 13 μA. When the operating frequency was increased from 2 Hz to 4 Hz, the output was further to 170V and 18 μA. In a separate study, BTO was doped into KNN without altering the orthorhombic lattice structure of KNN using a solid-state reaction that involved heating a mixture of solid reactants ($K_2CO_3$, $NaCO_3$, $BaCO_3$, $TiO_2$, and $Nb_2O_5$) to 1200 °C for 2 h [125]. The resulting BTO-KNN/PDMS PENG, prepared by spin-coating and poling, achieved a maximum output voltage of 58 V and a current of 0.45 μA under a 10 N load.

### 4.3. Doped carbon material-based nanofillers

In addition to perovskites, carbon-based materials have also been explored for doping in piezoelectric applications. Although doped carbon materials have been extensively studied for use in fuel cells, batteries, and supercapacitors [126], their application in PENGs remains relatively limited. Nitrogen doping has been employed to enhance the piezoelectric performance of carbon dot (CD)-based PENGs by promoting charge transfer and increasing surface defect density [127]. The N-doped CDs (N-CDs) are believed to promote β-phase formation in PVDF through electrostatic interactions with polymer chains, inducing the all-trans conformation. As a result, the N-CD/PVDF PENG achieved a maximum output voltage of 80 V and a current of 1.4 μA under a 12.3 N load at 6 Hz. In another study, p-type (B) and n-type (N) dopants were simultaneously introduced into reduced graphene oxide (rGO) to generate strong charge polarization within the carbon structure [128]. Under identical testing conditions (tapping at 6 Hz), the BN-rGO/PVDF PENG exhibited superior performance, producing an output voltage of 20.4 V and a current of 15.9 μA, outperforming both the N-rGO/PVDF (14.2 V, 8.7 μA) and pristine rGO/PVDF (12.4 V, 5.1 μA) counterparts. The piezoelectric nanocomposites based on doped perovskites and carbon materials are summarized in **Table 6**.

Doping nanofillers in piezoelectric nanocomposites can enhance their properties and performance by inducing lattice strain and distortion through ion substitution. This process improves the dielectric properties and surface polarization of the materials, leading to higher piezoelectric coefficients and increased energy conversion efficiency. These effects were demonstrated with V-ZnO and Y-ZnO nanofillers, which exhibited significant increases in $d_{33}$ values by 7 and 24 times, respectively, compared to their pristine ZnO counterparts. Overall, doping effectively enhanced the output performance of ZnO-based nanocomposites (**Table 5**).

**Table 5 •** Summary of piezoelectric nanocomposites based on doped ZnO nanofillers. The percentage values in parentheses indicate the increase in performance compared to nanocomposites with unmodified nanofillers.

| Ref. | Nanofiller | | | | | | | | Nanocomposite performance parameters | | | | |
|---|---|---|---|---|---|---|---|---|---|---|---|---|---|
| | Material | Shape | Diameter | $d_{33}$ (pC/N) | Nanofiller fraction | Polymer material | Fabrication method | Testing method | Voltage (V) | Current (μA) | $d_{33}$ (pC/N) | Power density (load) | Sensitivity (range) |
| [47] | Ag-ZnO | Sphere | ~150 nm | - | 30 wt% | PVDF-TrFE | Spin-coating, Annealing, Poling | Pressing (0.8 N at 1 Hz) | 2.04 (437% ↑) | - | - | - | - |
| [114] | Ba-ZnO | Rod | ~73 nm | 41.28 | 30 wt% | PDMS | Spin-coating | Pressing (~19.6 N at 1 Hz) | 10.5 (357% ↑) | - | - | - | 7.1 V/kgf ~0.72 V/N (0.75–2 kgf) |
| [107] | Ca-ZnO | Random | Random | - | 5 wt% | PVDF-TrFE | Solution casting | Pressing (0.5 N at 100 Hz) | 0.289 | - | - | - | ~0.3 V/N (0.05–0.5 N) |
| [104] | Co-ZnO | Rod | ~100 nm | - | 1 wt% | PVDF-HFP | Electrospinning | Pressing (2.5 N at 50 Hz) | 2.4 (1270% ↑) | - | - | - | - |
| [47] | Co-ZnO | Sphere | ~150 nm | - | 30 wt% | PVDF-TrFE | Spin-coating, Annealing, Poling | Pressing (0.8 N at 1 Hz) | 0.47 (24% ↑) | - | - | - | - |
| [105] | Fe-ZnO | Flowerlike | ~1.2 μm | - | 1 wt% | PVDF | Solution casting, γ-irradiation | Pressing (2.5 N at ~6 Hz) | 1.8 (125% ↑) | 0.016 | 8.29 (20% ↑) | 0.66 μW/cm² (1 MΩ) (224% ↑) | - |
| [106] | Fe-ZnO | Random | ~35 nm | - | 1 wt% | PVDF-TrFE | Solution casting | Finger tapping | 7 | - | - | - | - |
| [108] | La-ZnO | Rod | ~60 nm | - | 20 wt% | PDMS | Spin-coating | Pressing (2N) | 18 (260% ↑) | 0.1 (66% ↑) | - | 0.05 μW/cm² (100 MΩ) | - |
| [47] | Li-ZnO | Sphere | ~150 nm | - | 30 wt% | PVDF-TrFE | Spin-coating, Annealing, Poling | Pressing (0.8 N at 1 Hz) | 3.43 (800% ↑) | - | - | - | - |
| [47] | Na-ZnO | Sphere | ~150 nm | - | 30 wt% | PVDF-TrFE | Spin-coating, Annealing, Poling | Pressing (0.8 N at 1 Hz) | 1.87 (392% ↑) | - | - | - | - |
| [112] | Nd-ZnO | Rod | ~101 nm | 512 | 30 wt% | PDMS | Spin-coating | Finger tapping (~0.3 N) | ~31 (1450% ↑) | - | - | - | - |
| [113] | Tb-ZnO | Taper | ~100 nm | - | 30 wt% | PDMS | Spin-coating | Pressing (~19.6 N at 1 Hz) | 9 (291% ↑) | - | - | - | 6.53 V/kgf ~0.67 V/N (0.75–2 kgf) |
| [110] | V-ZnO | Flowerlike | ~5 μm | 65.5 (555% ↑) | - | BC | In situ synthesis, Poling | Bending | 1.5 | 0.08 | - | 0.06 μW/cm² (100 MΩ) | - |
| [111] | Y-ZnO | Sheet | ~34 nm (thickness) | ~420 (3287% ↑) | 30 wt% | PDMS | Spin-coating | Finger tapping (~0.98 N) | 20 (900% ↑) | - | - | - | - |

**Table 6 •** Summary of piezoelectric nanocomposites based on doped perovskites and carbon materials. The percentage values in parentheses indicate the increase in performance compared to nanocomposites with unmodified nanofillers.

| Ref. | Nanofiller | | | | | | | | Nanocomposite performance parameters | | | | |
|---|---|---|---|---|---|---|---|---|---|---|---|---|---|
| | **Material** | **Shape** | **Diameter** | **$d_{33}$ (pC/N)** | **Nanofiller fraction** | **Polymer material** | **Fabrication method** | **Testing method** | **Voltage (V)** | **Current (μA)** | **$d_{33}$ (pC/N)** | **Power density (load)** | **Sensitivity (range)** |
| [118] | Sr-BTO | Polyhedron | ~770 nm | - | 20 wt% | PVDF | Tape casting | Finger tapping (~10 N, 5 Hz) | 15 | - | ~50 | 6.75 μW/cm² (2 MΩ) | - |
| [117] | Ce-BTO | Fiber | 78.7 nm | ~9.5 (23% ↑) | 20 wt% | PVDF-TrFE | Electrospinning | Finger tapping | 0.29 | 0.36 | ~6.7 | 0.04 μW/cm² (100 MΩ) | - |
| [119] | Sr-BFO | Sphere | ~210 nm | - | 30 wt% | PDMS | Doctor blading | Pressing (10 N at 1 Hz) | 6.53 (110% ↑) | 0.64 (106% ↑) | - | 0.31 μW/cm² (100 MΩ) | - |
| [120] | Ba-BFO | Random | ~44 nm | - | 7 wt% | PVDF | Solution casting | Finger tapping | 20 (100% ↑) | 62.6 (272% ↑) | - | - | - |
| [122] | Ba/Zr-BFO | Sphere | ~44 nm | - | 15 wt% | PVDF | Solution casting, Poling | Finger tapping (~2.4 N at 5 Hz) | 30 | - | - | - | - |
| [123] | Sm/Ti-BFO | Random | ~400 nm | - | 30 wt% | Silicone rubber | Freeze drying, Doctor blading | Pressing (35 N at 1 Hz) | 5 (66% ↑) | 0.9 (50% ↑) | - | - | - |
| [124] | Al-$ZnSnO_3$ | Cube | 30–55 nm | - | 20 wt% | PDMS | Solution casting | Finger tapping (2 Hz) | 110 (120% ↑) | 13 (100% ↑) | | 120 μW/cm² (300% ↑) | - |
| [125] | BTO-KNN | Cube | ~100 | - | 10 wt% | PDMS | Spin-coating, Poling | Pressing (10 N) | 58 (45% ↑) | 0.45 (60% ↑) | - | 0.325 μW/cm² (10 MΩ) | - |
| [127] | N-CD | Sphere | 2.5 nm | - | 2.5 wt% | PVDF | Solution casting | Pressing (12.3 N at 6 Hz) | ~80 | ~1.4 | 29 | 9.1 μW/cm² (57 MΩ) | 10.2 V/kPa (≤ 0.5 kPa) |
| [128] | B/N-rGO | Sheet | - | - | - | PVDF | Solution casting | Pressing (6 Hz) | 20.4 (65% ↑) | 15.9 (212% ↑) | - | - | - |

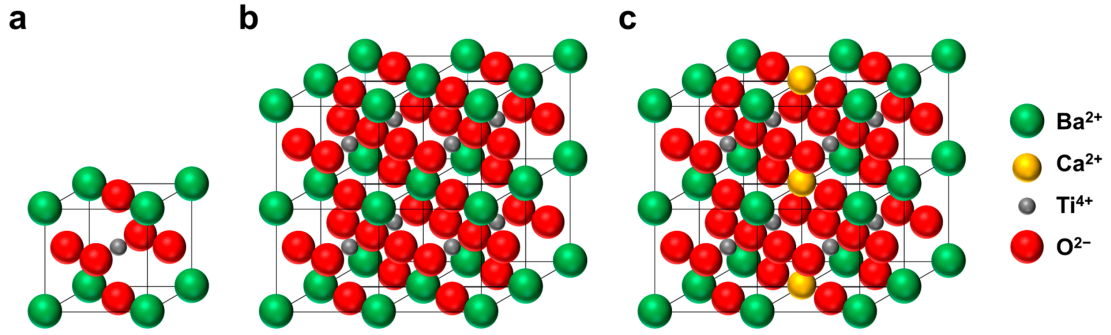


**Figure 13** • (**a**) A unit cell of an undistorted $ABO_3$ perovskite in a cubic structure, specifically for $BaTiO_3$; (**b**) 2 × 2 × 2 supercell of $BaTiO_3$; (**c**) 2 × 2 × 2 supercell of Ca-doped $BaTiO_3$ ($Ba_{0.75}Ca_{0.25}TiO_3$) in a tetragonal structure [115].

There appears to be more room for improvement in doping piezoelectric perovskites, as fewer studies have been reported compared to ZnO. Key design parameters for perovskites, such as the tolerance factor and octahedral factor, are commonly used to predict the stability of their 3D structures based on the ionic radii of each element. Additionally, the ionic valences of A and B sites and the coordination of B-site ions also affect the structure. These factors suggest significant potential for further research and optimization to improve the piezoelectric properties of doped perovskite nanocomposites [129].

## 5. Conclusions and outlook

Recent progress and efforts to improve the piezoelectric performance of polymer nanocomposites through nanofiller modification via surface coating, decoration, and chemical doping have been summarized, with a focus on sensing and nanogenerator applications. The effects of these modified nanofillers on output performance and their underlying processes are also discussed. The purpose of these modifications can be grouped into two categories: enhancing the piezoelectric properties of the nanofillers themselves and improving the interfacial interaction and stress transfer between the nanofillers and the polymer matrix. Coating with polymer materials aims to improve the dispersibility and compatibility of nanofillers within the polymer matrix, while coating or decorating with conductive materials enhances dipole alignment within the nanofillers under an applied electric field during electrospinning or poling. Doping is an effective method for enhancing the piezoelectricity of nanofillers by inducing lattice strain and distortion in the crystal structure, thereby improving the dielectric properties and surface polarization. All these modifications have demonstrated significant improvements in the output performance of polymer nanocomposites.

Future research would benefit from focusing more on comparing the local piezoelectric properties of individual nanofillers, typically obtained through PFM analysis, with the overall piezoelectric performance of the nanocomposite. This approach will provide a more comprehensive understanding of stress transferability within the composite. Given the limited number of studies reporting PFM data, caution is needed when drawing direct relationships. However, this method can offer critical insights into optimizing nanofiller–polymer interactions. Additionally, PFM data can help elucidate the effects of doping, as it directly observes the piezoelectricity of nanofillers, both before and after modification.

While most performance tests involve pressing nanocomposite films with a constant force, bending tests can offer more practical insights, particularly for applications involving vibrational motions from wind, buildings, and biomechanical activities. Including bending tests in evaluations is important to more accurately assess performances and to consider other piezoelectric coefficients, such as $d_{31}$, which relates polarization generated in the z-direction to stress applied in the x-direction.

Evaluating and improving the sensitivity of piezoelectric nanocomposite films is crucial, especially for applications that require a response to low applied stress levels. For instance, sensors designed to detect heartbeats need to respond to minimal changes in arterial diameter, typically in the order of hundreds of pascals or micrometers [130, 131]. This information suggests the importance of developing nanocomposites that can generate meaningful signals under low-stress conditions, making them suitable for biomechanical applications.

To enhance the utility of power density as a parameter, establishing standardized criteria for its evaluation is necessary. Currently, numerous research articles report power density values obtained under various conditions and emphasize the maximum value, making it difficult to draw meaningful conclusions. Standardization would facilitate more accurate comparisons and advancements in this field.

Exploring the combination of surface coating/decorating with chemical doping of nanofillers, such as doped nanofillers coated with polymers, is worth considering as this approach could create synergistic effects on the nanocomposites. As improvements from each modification are observed, investigating how these combined modifications affect overall performance can lead to innovative approaches for optimizing piezoelectric properties.

Hybrid nanogenerators that combine multiple processes offer a promising advancement in energy-harvesting technology by leveraging the complementary strengths of each process to achieve higher efficiency and broader applicability. For example, the output performance of the B/N-rGO/PVDF nanocomposite significantly improved when a PDMS layer was added on top to induce a triboelectric effect, facilitating contact between them (**Figure 14**). This piezo–tribo hybrid nanogenerator further increased the output voltage and current to 57.6 V (a 182% increase) and 28.8 μA (a 77% increase), respectively [128]. Several other studies have also demonstrated the potential of piezo–tribo hybrid systems [132–134]. These hybrid systems can capture a wider

range of mechanical stimuli, including vibrations, pressure, friction, and motion, thereby enhancing overall energy-conversion efficiency. While challenges such as material compatibility, device integration, and long-term stability remain, continued research and development can address these issues and unlock innovative solutions for sustainable energy generation.

Alongside these approaches, concerted efforts should focus on developing novel piezoelectric materials that can complement nanofiller modification strategies and further advance the performance, flexibility, and functionality of next-generation energy harvesting devices. In recent years, new classes of piezoelectric materials have emerged as promising alternatives to conventional ceramics and polymers. Among these, 2D materials such as $MoS_2$, $WS_2$, and MXenes have attracted significant interest due to their unique structural and electronic characteristics. Their atomically thin nature provides high mechanical flexibility and a large surface area, which can enhance interfacial interactions when embedded in polymer matrices. Notably, symmetry breaking in monolayer 2D materials enables piezoelectricity that is absent in their bulk forms, making them suitable for applications in flexible and wearable nanogenerators [135–137]. Metal–organic frameworks (MOFs) represent another emerging group of piezoelectric materials. These materials offer structural tunability through the combination of inorganic metal centers and organic ligands. MOFs are typically lightweight, porous, and compressible, which can be advantageous for low-pressure or skin-conformal energy harvesting devices. Their abundance of functional groups facilitates compatibility with polymer matrices and supports diverse surface functionalization strategies [138–141]. However, these materials often exhibit lower mechanical stability and are sensitive to environmental factors such as humidity and oxidation, and challenges remain in achieving scalable synthesis and consistent device integration [142, 143]. While established materials such as PVDF, ZnO, and BTO remain dominant due to their high piezoelectric performance and well-characterized processing methods, 2D materials and MOFs provide unique advantages in terms of flexibility, tunability, and functional integration. The continued exploration of these emerging materials may lead to the development of next-generation nanogenerators for flexible and multifunctional energy-harvesting applications.

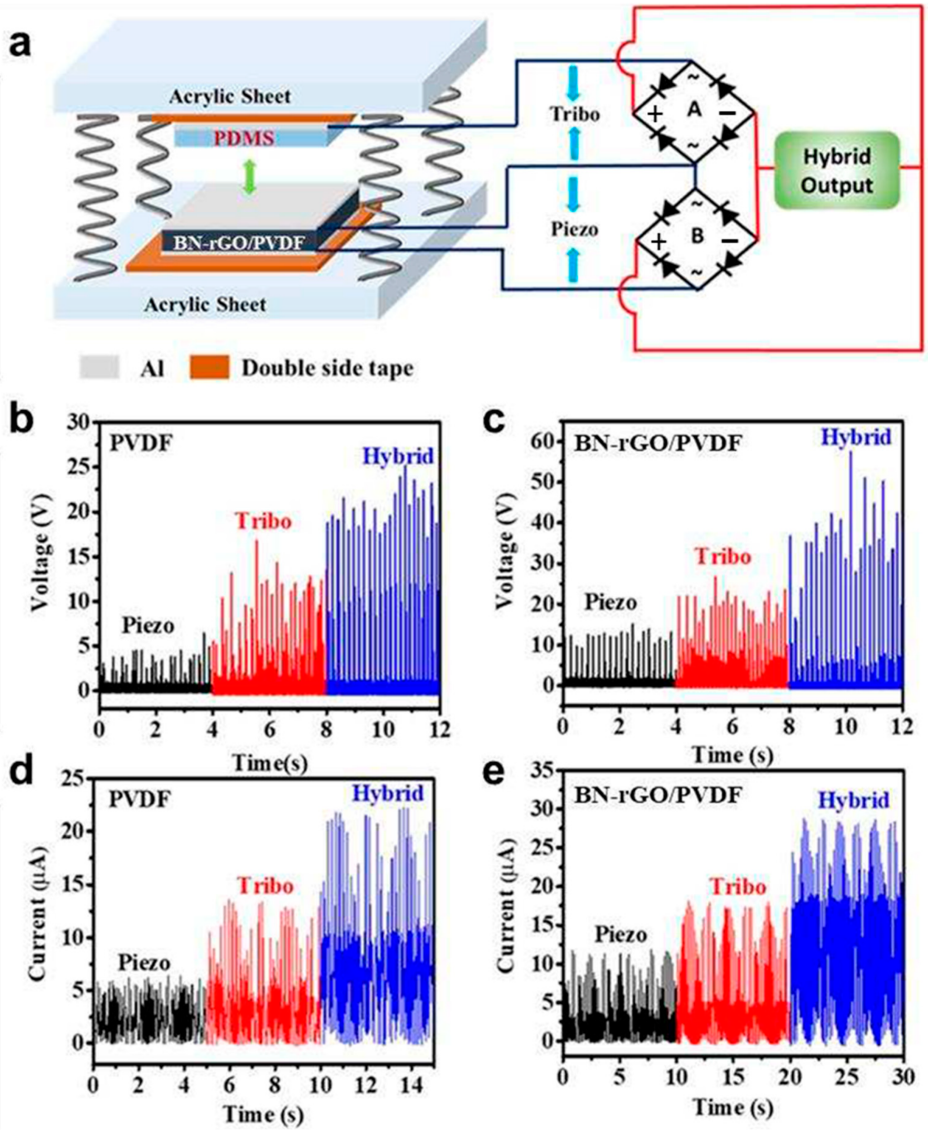


**Figure 14** • (**a**) Schematic representation of the piezo–tribo hybrid nanogenerator. (**b**,**c**) Comparison of the voltages and (**d**,**e**) comparison of the currents from piezo, tribo, and hybrid nanogenerators based on PVDF and BN-rGO/PVDF composite films. Reproduced with permission from [128]. Copyright 2022, American Chemical Society.

## Funding

This work was supported by the Air Force Office of Scientific Research [AFOSR FA9550-23-1-0581; 23RT0567] and the Robert A. Welch Foundation [E-1320 and V-E-0001].

## Author contributions

Conceptualization, J.M.L. and T.R.L.; methodology, J.M.L. and T.R.L.; software, T.R.L.; validation, J.M.L.; formal analysis, J.M.L.; investigation, J.M.L.; resources, J.M.L. and T.R.L.; data curation, J.M.L.; writing—original draft preparation, J.M.L.; writing—review and editing, H.V.T., P.C., and T.R.L.; visualization, J.M.L.; supervision, T.R.L.; project administration, J.M.L., H.V.T., and P.C.; funding acquisition, T.R.L. All authors have read and agreed to the published version of the manuscript.

## Conflicts of interest

The authors declare that they have no competing interests.

## Data availability statement

All data supporting the findings of this publication are available within this article.

## Additional information

Received: 2025-05-27

Accepted: 2025-07-22

Published: 2025-07-31

*Academia Nano: Science, Materials, Technology* papers should be cited as *Academia Nano: Science, Materials, Technology 2025*, ISSN 3065-9736, https://doi.org/10.20935/AcadNano7835. The journal's official abbreviation is *Acad. Nano: Sci. Mat. Tech.*

## Publisher's note



## Copyright



## References

1. Harb A. Energy harvesting: state-of-the-art. Renew Energy. 2011;36:2641–54. doi: 10.1016/j.renene.2010.06.014
2. Wang H, Jasim A, Chen X. Energy harvesting technologies in roadway and bridge for different applications—a comprehensive review. Appl Energy. 2018;212:1083–94. doi: 10.1016/j.apenergy.2017.12.125
3. Hao D, Qi L, Tairab AM, Ahmed A, Azam A, Luo D, et al. Solar energy harvesting technologies for PV self-powered applications: a comprehensive review. Renew Energy. 2022;188:678–97. doi: 10.1016/j.renene.2022.02.066
4. Kim KA, Bagci FS, Dorsey KL. Design considerations for photovoltaic energy harvesting in wearable devices. Sci Rep. 2022;12:18143. doi: 10.1038/s41598-022-22232-x
5. Mondal R, Hasan MAM, Baik JM, Yang Y. Advanced pyroelectric materials for energy harvesting and sensing applications. Mater Today. 2023;66:273–301. doi: 10.1016/j.mattod.2023.03.023
6. Panda S, Hajra S, Song H, Jo J, Kim N, Hwang S, et al. Pyroelectric based energy harvesting devices: hybrid structures and applications. Sustain Energy Fuels. 2023;7:5319–35. doi: 10.1039/D3SE01180A
7. Tian J, Chen X, Wang ZL. Environmental energy harvesting based on triboelectric nanogenerators. Nanotechnology. 2020;31:242001. doi: 10.1088/1361-6528/ab793e
8. Zou Y, Raveendran V, Chen J. Wearable triboelectric nanogenerators for biomechanical energy harvesting. Nano Energy. 2020;77:105303. doi: 10.1016/j.nanoen.2020.105303
9. Ho DH, Han J, Huang J, Choi YY, Cheon S, Sun J, et al. β-phase-preferential blow-spun fabrics for wearable triboelectric nanogenerators and textile interactive interface. Nano Energy. 2020;77:105262. doi: 10.1016/j.nanoen.2020.105262
10. Miao G, Fang S, Wang S, Zhou S. A low-frequency rotational electromagnetic energy harvester using a magnetic plucking mechanism. Appl Energy. 2022;305:117838. doi: 10.1016/j.apenergy.2021.117838
11. Carneiro P, Soares dos Santos MP, Rodrigues A, Ferreira JAF, Simões JAO, Marques AT, et al. Electromagnetic energy harvesting using magnetic levitation architectures: a review. Appl Energy. 2020;260:114191. doi: 10.1016/j.apenergy.2019.114191
12. Huang Q, Jiang Y, Duan Z, Wu Y, Yuan Z, Guo J, et al. Ion gradient induced self-powered flexible strain sensor. Nano Energy. 2024;126:109689. doi: 10.1016/j.nanoen.2024.109689
13. Huang Q, Jiang Y, Duan Z, Wu Y, Yuan Z, Zhang M, et al. Electrochemical self-powered strain sensor for static and dynamic strain detections. Nano Energy. 2023;118:108997. doi: 10.1016/j.nanoen.2023.108997

14. Duan Z, Zhang B, Zhang M, Yuan Z, Jiang Y, Tai H. High-performance electrochemical power generation humidity sensor based on NaCl/sodium alginate humidity sensing electrolyte and Cu/Zn electrodes for visual humidity indication and respiratory patterns detection. Sens Actuators B Chem. 2024;409:135585. doi: 10.1016/j.snb.2024.135585

15. Zu Y, Hu J, Yang M, Duan Z, Zhang M, Yuan Z, et al. Electrochemical power generation humidity sensor based on WS2 nanoflakes. Sens Actuators B Chem. 2024;405:135325. doi: 10.1016/j.snb.2024.135325

16. Huang Q, Jiang Y, Duan Z, Wu Y, Yuan Z, Zhang M, et al. Ion gradient induced self-powered flexible pressure sensor. Chem Eng J. 2024;490:151660. doi: 10.1016/j.cej.2024.151660

17. Liu B, Jiang Y, Xie G, Duan Z, Yuan Z, Zhang Y, et al. Lever-inspired triboelectric respiration sensor for respiratory behavioral assessment and exhaled hydrogen sulfide detection. Chem Eng J. 2023;471:144795. doi: 10.1016/j.cej.2023.144795

18. Habib M, Lantgios I, Hornbostel K. A review of ceramic, polymer and composite piezoelectric materials. J Phys D: Appl Phys. 2022;55:423002. doi: 10.1088/1361-6463/ac8687

19. Smith M, Kar-Narayan S. Piezoelectric polymers: theory, challenges and opportunities. Int Mater Rev. 2022;67:65–88. doi: 10.1080/09506608.2021.1915935

20. Mohammadpourfazeli S, Arash S, Ansari A, Yang S, Mallick K, Bagherzadeh R. Future prospects and recent developments of polyvinylidene fluoride (PVDF) piezoelectric polymer; fabrication methods, structure, and electromechanical properties. RSC Adv. 2022;13:370–87. doi: 10.1039/D2RA06774A

21. Malakooti MH, Sodano HA. Piezoelectric energy harvesting through shear mode operations. Smart Mater Struct. 2015;24:055005. doi: 10.1088/0964-1726/24/5/055005

22. Jella V, Ippili S, Eom JH, Pammi SVN, Jung JS, Tran VD, et al. A comprehensive review of flexible piezoelectric generators based on organic-inorganic metal halide perovskites. Nano Energy. 2019;57:74–93. doi: 10.1016/j.nanoen.2018.12.038

23. Khatua DK, Kim SJ. Perspective on the development of high performance flexible piezoelectric energy harvesters. J Mater Chem C. 2022;10:2905–24. doi: 10.1039/D1TC06089A

24. Liu X, Shang Y, Zhang J, Zhang C. Ionic liquid-assisted 3D printing of self-polarized β-PVDF for flexible piezoelectric energy harvesting. ACS Appl Mater Interfaces. 2021;13:14334–41. doi: 10.1021/acsami.1c03226

25. Fu J, Hou Y, Zheng M, Zhu M. Flexible piezoelectric energy harvester with extremely high power generation capability by sandwich structure design strategy. ACS Appl Mater Interfaces. 2020;12:9766–74. doi: 10.1021/acsami.9b21201

26. Khan MB, Kim DH, Han JH, Saif H, Lee H, Lee Y, et al. Performance improvement of flexible piezoelectric energy harvester for irregular human motion with energy extraction enhancement circuit. Nano Energy. 2019;58:211–9. doi: 10.1016/j.nanoen.2019.01.049

27. Liu H, Zhong J, Lee C, Lee SW, Lin L. A comprehensive review on piezoelectric energy harvesting technology: materials, mechanisms, and applications. Appl Phys Rev. 2018;5:041306. doi: 10.1063/1.5074184

28. Hao J, Li W, Zhai J, Chen H. Progress in high-strain perovskite piezoelectric ceramics. Mater Sci Eng R Rep. 2019;135:1–57. doi: 10.1016/j.mser.2018.08.001

29. Zaszczyńska A, Gradys A, Sajkiewicz P. Progress in the applications of smart piezoelectric materials for medical devices. Polymers. 2020;12:2754. doi: 10.3390/polym12112754

30. Wu J. Perovskite lead-free piezoelectric ceramics. J Appl Phys. 2020;127:190901. doi: 10.1063/5.0006261

31. Sappati KK, Bhadra S. Piezoelectric polymer and paper substrates: a review. Sensors. 2018;18:3605. doi: 10.3390/s18113605

32. Chamankar N, Khajavi R, Yousefi AA, Rashidi A, Golestanifard F. A flexible piezoelectric pressure sensor based on PVDF nanocomposite fibers doped with PZT particles for energy harvesting applications. Ceram Int. 2020;46:19669–81. doi: 10.1016/j.ceramint.2020.03.210

33. Jiang J, Tu S, Fu R, Li J, Hu F, Yan B, et al. Flexible piezoelectric pressure tactile sensor based on electrospun $BaTiO_3$/poly(vinylidene fluoride) nanocomposite membrane. ACS Appl Mater Interfaces. 2020;12:33989–98. doi: 10.1021/acsami.0c08560

34. Kim HJ, Kim YJ. High performance flexible piezoelectric pressure sensor based on CNTs-doped 0–3 ceramic-epoxy nanocomposites. Mater Des. 2018;151:133–40. doi: 10.1016/j.matdes.2018.04.048

35. Sodagar S, Jaleh B, Fakhri P, Kashfi M, Mohazzab BF, Momeni A. Flexible piezoelectric PVDF/NDs nanocomposite films: improved electroactive properties at low concentration of nanofiller and numerical simulation using finite element method. J Polym Res. 2020;27:203. doi: 10.1007/s10965-020-02184-4

36. Muthusamy L, Uppalapati B, Azad S, Bava M, Koley G. Self-poled P(VDF-TrFE)/carbon black composite piezoelectric thin film. Polymers. 2023;15:4131. doi: 10.3390/polym15204131

37. Choudhry I, Khalid HR, Lee HK. Flexible piezoelectric transducers for energy harvesting and sensing from human kinematics. ACS Appl Electron Mater. 2020;2:3346–57. doi: 10.1021/acsaelm.0c00636

38. Zhai W, Lai Q, Chen L, Zhu L, Wang ZL. Flexible piezoelectric nanogenerators based on P(VDF–TrFE)/GeSe nanocomposite films. ACS Appl Electron Mater. 2020;2:2369–74. doi: 10.1021/acsaelm.0c00525

39. Bhagavathula SD, Kokkarachedu V, Acuna DQ, Koduri R, Veluri S, Reddy V. Insight of electrical behavior in ferroelectric-semiconductor polymer nanocomposite films of PVDF/ZnSe and PVDF/Cu:ZnSe. J Appl Polym Sci. 2017;134:44983. doi: 10.1002/app.44983

40. Wu B, Yang Y, Wang L, Xu H, Huang Y, Kang J, et al. $SnO_2$ induced electrostatic polarization PVDF composite nanofibers for efficient energy harvesting and self-powered wireless monitoring/motion recognition systems. Chem Eng J. 2024;495:153483. doi: 10.1016/j.cej.2024.153483

41. Ekbote GS, Khalifa M, Mahendran A, Anandhan S. Cationic surfactant assisted enhancement of dielectric and piezoelectric properties of PVDF nanofibers for energy harvesting application. Soft Matter. 2021;17:2215–22. doi: 10.1039/D0SM01943G

42. Sobola D, Kaspar P, Částková K, Dallaev R, Papež N, Sedlák P, et al. PVDF fibers modification by nitrate salts doping. Polymers. 2021;13:2439. doi: 10.3390/polym13152439

43. Lund A, Gustafsson C, Bertilsson H, Rychwalski RW. Enhancement of β phase crystals formation with the use of nanofillers in PVDF films and fibres. Compos Sci Technol. 2011;71:222–9. doi: 10.1016/j.compscitech.2010.11.014

44. Choi MH, Yang SC. $CoFe_2O_4$ nanofiller effect on β-phase formation of PVDF matrix for polymer-based magnetoelectric composites. Mater Lett. 2018;223:73–77. doi: 10.1016/j.matlet.2018.04.024

45. Zhang Y, Kim H, Wang Q, Jo W, Kingon AI, Kim SH, et al. Progress in lead-free piezoelectric nanofiller materials and related composite nanogenerator devices. Nanoscale Adv. 2020;2:3131–49. doi: 10.1039/C9NA00809H

46. Su Y, Li W, Yuan L, Chen C, Pan H, Xie G, et al. Piezoelectric fiber composites with polydopamine interfacial layer for self-powered wearable biomonitoring. Nano Energy. 2021;89:106321. doi: 10.1016/j.nanoen.2021.106321

47. Jin C, Hao N, Xu Z, Trase I, Nie Y, Dong L, et al. Flexible piezoelectric nanogenerators using metal-doped ZnO-PVDF films. Sens Actuators A Phys. 2020;305:111912. doi: 10.1016/j.sna.2020.111912

48. Tang H, Wang P, Zheng P, Liu X. Core-shell structured $BaTiO_3$@polymer hybrid nanofiller for poly(arylene ether nitrile) nanocomposites with enhanced dielectric properties and high thermal stability. Compos Sci Technol. 2016;123:134–42. doi: 10.1016/j.compscitech.2015.12.015

49. Yang Y, Pan H, Xie G, Jiang Y, Chen C, Su Y, et al. Flexible piezoelectric pressure sensor based on polydopamine-modified $BaTiO_3$/PVDF composite film for human motion monitoring. Sens Actuators A Phys. 2020;301:111789. doi: 10.1016/j.sna.2019.111789

50. Su Y, Chen C, Pan H, Yang Y, Chen G, Zhao X, et al. Muscle fibers inspired high-performance piezoelectric textiles for wearable physiological monitoring. Adv Funct Mater. 2021;31:2010962. doi: 10.1002/adfm.202010962

51. Guan X, Xu B, Gong J. Hierarchically architected polydopamine modified $BaTiO_3$@P(VDF-TrFE) nanocomposite fiber mats for flexible piezoelectric nanogenerators and self-powered sensors. Nano Energy. 2020;70:104516. doi: 10.1016/j.nanoen.2020.104516

52. Wang L, Cheng T, Lian W, Zhang M, Lu B, Dong B, et al. Flexible layered cotton cellulose-based nanofibrous membranes for piezoelectric energy harvesting and self-powered sensing. Carbohydr Polym. 2022;275:118740. doi: 10.1016/j.carbpol.2021.118740

53. Wan X, Wang Z, Zhao X, Hu Q, Li Z, Wang ZL, et al. Flexible and highly piezoelectric nanofibers with organic–inorganic coaxial structure for self-powered physiological multimodal sensing. Chem Eng J. 2023;451:139077. doi: 10.1016/j.cej.2022.139077

54. Hanani Z, Izanzar I, Amjoud M, Mezzane D, Lahcini M, Uršič H, et al. Lead-free nanocomposite piezoelectric nanogenerator film for biomechanical energy harvesting. Nano Energy. 2021;81:105661. doi: 10.1016/j.nanoen.2020.105661

55. Hanani Z, Izanzar I, Merselmiz S, Assimi TE, Mezzane D, Amjoud M, et al. A flexible self-poled piezocomposite nanogenerator based on H2(Zr0.1Ti0.9)3O7 nanowires and polylactic acid biopolymer. Sustain Energy Fuels. 2022;6:1983–91. doi: 10.1039/D2SE00234E

56. Mayeen A, Kala MS, Jayalakshmy MS, Thomas S, Rouxel D, Philip J, et al. Dopamine functionalization of $BaTiO_3$: an effective strategy for the enhancement of electrical, magnetoelectric and thermal properties of $BaTiO_3$-PVDF-TrFE nanocomposites. Dalton Trans. 2018;47:2039–51. doi: 10.1039/C7DT03389C

57. Sada T, Ndayishimiye A, Fan Z, Fujioka Y, Randall CA. Surface modification of $BaTiO_3$ with catechol surfactant and effects on cold sintering. J Appl Phys. 2021;129:184102. doi: 10.1063/5.0049905

58. Li H, Lim S. Boosting performance of self-polarized fully printed piezoelectric nanogenerators via modulated strength of hydrogen bonding interactions. Nanomaterials. 2021;11:1908. doi: 10.3390/nano11081908

59. Mishra S, Unnikrishnan L, Nayak SK, Mohanty S. Advances in piezoelectric polymer composites for energy harvesting applications: a systematic review. Macromol Mater Eng. 2019;304:1800463. doi: 10.1002/mame.201800463

60. Li X, Chen S, Zhang X, Li J, Liu H, Han N, et al. Poly-L-lactic acid/graphene electrospun composite nanofibers for wearable sensors. Energy Technol. 2020;8:1901252. doi: 10.1002/ente.201901252

61. Chen TP, Liu T, Su TL, Liang J. Self-polymerization of dopamine in acidic environments without oxygen. Langmuir. 2017;33:5863–71. doi: 10.1021/acs.langmuir.7b01127

62. Cho Y, Jeong J, Choi M, Baek G, Park S, Choi H, et al. $BaTiO_3$@PVDF-TrFE nanocomposites with efficient orientation prepared via phase separation nano-coating method for piezoelectric performance improvement and application

to 3D-PENG. Chem Eng J. 2022;427:131030. doi: 10.1016/j.cej.2021.131030

63. Shi K, Chai B, Zou H, Shen P, Sun B, Jiang P, et al. Interface induced performance enhancement in flexible $BaTiO_3$/PVDF-TrFE based piezoelectric nanogenerators. Nano Energy. 2021;80:105515. doi: 10.1016/j.nanoen.2020.105515

64. Parangusan H, Bhadra J, Al-Thani N. Flexible piezoelectric nanogenerator based on [P(VDF-HFP)]/PANI-ZnS electrospun nanofibers for electrical energy harvesting. J Mater Sci: Mater Electron. 2021;32:6358–68. doi: 10.1007/s10854-021-05352-4

65. Majhi M, Choudhary RB, Maji P. HCl protonated polymeric PANI-ZnS nanocomposites and measurement of their robust dielectric, optical and thermal performance. Optik. 2017;136:181–91. doi: 10.1016/j.ijleo.2017.02.015

66. Zhao B, Chen Z, Cheng Z, Wang S, Yu T, Yang W, et al. Piezoelectric nanogenerators based on electrospun PVDF-coated mats composed of multilayer polymer-coated $BaTiO_3$ nanowires. ACS Appl Nano Mater. 2022;5:8417–28. doi: 10.1021/acsanm.2c01538

67. Xie L, Huang X, Huang Y, Yang K, Jiang P. Core@double-shell structured $BaTiO_3$–polymer nanocomposites with high dielectric constant and low dielectric loss for energy storage application. J Phys Chem C. 2013;117:22525–37. doi: 10.1021/jp407340n

68. Han Y, Jiang C, Lin H, Luo C, Qi R, Peng H. Piezoelectric nanogenerators based on helical carbon materials and polyvinyledenedifluoride–trifluoroethylene hybrids with enhanced energy-harvesting performance. Energy Technol. 2020;8:1901249. doi: 10.1002/ente.201901249

69. Yang J, Zhang Y, Li Y, Wang Z, Wang W, An Q, et al. Piezoelectric nanogenerators based on graphene oxide/PVDF electrospun nanofiber with enhanced performances by in-situ reduction. Mater Today Commun. 2021;26:101629. doi: 10.1016/j.mtcomm.2020.101629

70. Shi K, Sun B, Huang X, Jiang P. Synergistic effect of graphene nanosheet and $BaTiO_3$ nanoparticles on performance enhancement of electrospun PVDF nanofiber mat for flexible piezoelectric nanogenerators. Nano Energy. 2018;52:153–62. doi: 10.1016/j.nanoen.2018.07.053

71. Li L, Guo H, Sun H, Sui H, Yang X, Wang F, et al. The construction of $BaTiO_3$-based core-shell composites for high-performance and flexible piezoelectric nanogenerators. Sens Actuators A Phys. 2023;363:114553. doi: 10.1016/j.sna.2023.114553

72. Zhou Z, Zhang Z, Zhang Q, Yang H, Zhu Y, Wang Y, et al. Controllable core–shell $BaTiO_3$@carbon nanoparticle-enabled P(VDF-TrFE) composites: a cost-effective approach to high-performance piezoelectric nanogenerators. ACS Appl Mater Interfaces. 2020;12:1567–76. doi: 10.1021/acsami.9b18780

73. Zhou Z, Du X, Zhang Z, Luo J, Niu S, Shen D, et al. Interface modulated 0-D piezoceramic nanoparticles/PDMS based piezoelectric composites for highly efficient energy harvesting application. Nano Energy. 2021;82:105709. doi: 10.1016/j.nanoen.2020.105709

74. Qi F, Zeng Z, Yao J, Cai W, Zhao Z, Peng S, et al. Constructing core-shell structured $BaTiO_3$@carbon boosts piezoelectric activity and cell response of polymer scaffolds. Mater Sci Eng C. 2021;126:112129. doi: 10.1016/j.msec.2021.112129

75. Li X, Ji D, Yu B, Ghosh R, He J, Qin X, et al. Boosting piezoelectric and triboelectric effects of PVDF nanofiber through carbon-coated piezoelectric nanoparticles for highly sensitive wearable sensors. Chem Eng J. 2021;426:130345. doi: 10.1016/j.cej.2021.130345

76. You I, Jeon H, Lee K, Do M, Seo YC, Lee HA, et al. Polydopamine coating in organic solvent for material-independent immobilization of water-insoluble molecules and avoidance of substrate hydrolysis. J Ind Eng Chem. 2017;46:379–85. doi: 10.1016/j.jiec.2016.11.007

77. Kim Y, Kim H, Lee GJ, Lee HU, Lee SG, Baek C, et al. Flexoelectric-boosted piezoelectricity of $BaTiO_3$@$SrTiO_3$ core-shell nanostructure determined by multiscale simulations for flexible energy harvesters. Nano Energy. 2021;89:106469. doi: 10.1016/j.nanoen.2021.106469

78. Yudin PV, Tagantsev AK. Fundamentals of flexoelectricity in solids. Nanotechnology. 2013;24:432001. doi: 10.1088/0957-4484/24/43/432001

79. Nguyen TD, Mao S, Yeh YW, Purohit PK, McAlpine MC. Nanoscale flexoelectricity. Adv Mater. 2013;25:946–74. doi: 10.1002/adma.201203852

80. Samadi A, Pourahmad S. Flexible piezoelectric cum-electromagnetic-absorbing multifunctional nanocomposites based on electrospun poly (vinylidene fluoride) incorporated with synthesized porous core-shell nanoparticles. Int J Energy Res. 2020;44:10087–100. doi: 10.1002/er.5623

81. Luo J, Pan S, Cheng L, Lin P, He Y, Chang J. Electromagnetic and microwave absorption properties of Er-Ho-Fe alloys. J Rare Earths. 2018;36:715–20. doi: 10.1016/j.jre.2018.02.006

82. Kang JH, Jeong DK, Ryu SW. Transparent, flexible piezoelectric nanogenerator based on GaN membrane using electrochemical lift-off. ACS Appl Mater Interfaces. 2017;9:10637–42. doi: 10.1021/acsami.6b15587

83. Johar MA, Hassan MA, Waseem A, Ha JS, Lee JK, Ryu SW. Stable and high piezoelectric output of GaN nanowire-based lead-free piezoelectric nanogenerator by suppression of internal screening. Nanomaterials. 2018;8:437. doi: 10.3390/nano8060437

84. Waseem A, Johar MA, Hassan MA, Bagal IV, Ha JS, Lee JK, et al. Effect of crystal orientation of GaN/V2O5 core-shell nanowires on piezoelectric nanogenerators. Nano Energy. 2019;60:413–23. doi: 10.1016/j.nanoen.2019.03.075

85. Waseem A, Johar MA, Hassan MA, Bagal IV, Ha JS, Lee JK, et al. GaN/$Al_2O_3$ core-shell nanowire based flexible and stable piezoelectric energy harvester. J Alloys Compd. 2021;860:158545. doi: 10.1016/j.jallcom.2020.158545

86. Xia Y, Qian W, Yang Y. Advancements and prospects of flexoelectricity. ACS Appl Mater Interfaces. 2024;16:9597–613. doi: 10.1021/acsami.3c16727

87. Ma Y, Liu M, Feng Y, Zheng H, Wu Y. ZnO@Ag modified piezoelectric fibers for higher sensitivity and enhanced energy harvesting. J Mater Res Technol. 2022;20:2689–704. doi: 10.1016/j.jmrt.2022.08.067

88. Yan M, Liu S, Liu Y, Xiao Z, Yuan X, Zhai D, et al. Flexible PVDF–TrFE nanocomposites with Ag-decorated BCZT heterostructures for piezoelectric nanogenerator applications. ACS Appl Mater Interfaces. 2022;14:53261–73. doi: 10.1021/acsami.2c15581

89. Kar E, Bose N, Dutta B, Mukherjee N, Mukherjee S. MWCNT@$SiO_2$ heterogeneous nanofiller-based polymer composites: a single key to the high-performance piezoelectric nanogenerator and X-band microwave shield. ACS Appl Nano Mater. 2018;1:4005–18. doi: 10.1021/acsanm.8b00770

90. Khalifa M, Peravali S, Varsha S, Anandhan S. Piezoelectric energy harvesting using flexible self-poled electroactive nanofabrics based on PVDF/ZnO-decorated SWCNT nanocomposites. JOM. 2022;74:3162–71. doi: 10.1007/s11837-022-05342-9

91. Bhat AR, Pratihar S, Manzoor S, Chandran AM, Yella A, Mural PKS. Augmenting piezoelectric performance of poly (vinylidene fluoride) nanogenerator with zinc oxide nanorods decorated reduced graphene oxide nanosheets. ACS Appl Nano Mater. 2024;7:10268–83. doi: 10.1021/acsanm.4c00732

92. Badatya S, Kumar A, Srivastava AK, Gupta MK. Flexible interconnected Cu-Ni nanoalloys decorated carbon nanotube-poly(vinylidene fluoride) piezoelectric nanogenerator. Adv Mater Technol. 2022;7:2101281. doi: 10.1002/admt.202101281

93. Shim J, Son DI, Lee JS, Lee J, Lim GH, Cho H, et al. BNNT-ZnO QDs nanocomposites for improving piezoelectric nanogenerator and piezoelectric properties of boron nitride nanotube. Nano Energy. 2022;93:106886. doi: 10.1016/j.nanoen.2021.106886

94. Shuai C, Liu G, Yang Y, Qi F, Peng S, Yang W, et al. A strawberry-like Ag-decorated barium titanate enhances piezoelectric and antibacterial activities of polymer scaffold. Nano Energy. 2020;74:104825. doi: 10.1016/j.nanoen.2020.104825

95. Lei Y, Xu S, Ding M, Li L, Sun Q, Wang ZL. Enhanced photocatalysis by synergistic piezotronic effect and exciton–plasmon interaction based on (Ag-Ag2S)/$BaTiO_3$ heterostructures. Adv Funct Mater. 2020;30:2005716. doi: 10.1002/adfm.202005716

96. Xu S, Guo L, Sun Q, Wang ZL. Piezotronic effect enhanced plasmonic photocatalysis by AuNPs/$BaTiO_3$ heterostructures. Adv Funct Mater. 2019;29:1808737. doi: 10.1002/adfm.201808737

97. Guo L, Zhong C, Cao J, Hao Y, Lei M, Bi K, et al. Enhanced photocatalytic $H_2$ evolution by plasmonic and piezotronic effects based on periodic Al/$BaTiO_3$ heterostructures. Nano Energy. 2019;62:513–20. doi: 10.1016/j.nanoen.2019.05.067

98. Medhi R, Marquez MD, Lee TR. Visible-light-active doped metal oxide nanoparticles: review of their synthesis, properties, and applications. ACS Appl Nano Mater. 2020;3:6156–85. doi: 10.1021/acsanm.0c01035

99. Maldonado F, Stashans A. Al-doped ZnO: electronic, electrical and structural properties. J Phys Chem Solids. 2010;71:784–7. doi: 10.1016/j.jpcs.2010.02.001

100. Hu D, Yao M, Fan Y, Ma C, Fan M, Liu M. Strategies to achieve high performance piezoelectric nanogenerators. Nano Energy. 2019;55:288–304. doi: 10.1016/j.nanoen.2018.10.053

101. Pandey RK, Dutta J, Brahma S, Rao B, Liu CP. Review on ZnO-based piezotronics and piezoelectric nanogenerators: aspects of piezopotential and screening effect. J Phys Mater. 2021;4:044011. doi: 10.1088/2515-7639/ac130a

102. Cao X, Xiong Y, Sun J, Zhu X, Sun Q, Wang ZL. Piezoelectric nanogenerators derived self-powered sensors for multifunctional applications and artificial intelligence. Adv Funct Mater. 2021;31:2102983. doi: 10.1002/adfm.202102983

103. Le AT, Ahmadipour M, Pung SY. A review on ZnO-based piezoelectric nanogenerators: synthesis, characterization techniques, performance enhancement and applications. J Alloys Compd. 2020;844:156172. doi: 10.1016/j.jallcom.2020.156172

104. Parangusan H, Ponnamma D, Al-Maadeed MAA. Stretchable electrospun PVDF-HFP/Co-ZnO nanofibers as piezoelectric nanogenerators. Sci Rep. 2018;8:754. doi: 10.1038/s41598-017-19082-3

105. Parangusan H, Ponnamma D, Al-Maadeed MAA. Investigation on the effect of $\gamma$-irradiation on the dielectric and piezoelectric properties of stretchable PVDF/Fe–ZnO nanocomposites for self-powering devices. Soft Matter. 2018;14:8803–13. doi: 10.1039/C8SM01655K

106. Sahoo R, Mishra S, Unnikrishnan L, Mohanty S, Mahapatra S, Nayak SK, et al. Enhanced dielectric and piezoelectric properties of Fe-doped ZnO/PVDF-TrFE composite films. Mater Sci Semicond Process. 2020;117:105173. doi: 10.1016/j.mssp.2020.105173

107. Sahoo R, Mishra S, Ramadoss A, Mohanty S, Mahapatra S, Nayak SK. An approach towards the fabrication of energy harvesting device using Ca-doped ZnO/PVDF-TrFE composite film. Polymer. 2020;205:122869. doi: 10.1016/j.polymer.2020.122869

108. Pandey R, Khandelwal G, Palani IA, Singh V, Kim SJ. A La-doped ZnO ultra-flexible flutter-piezoelectric nanogenerator for energy harvesting and sensing applications: a novel renewable source of energy. Nanoscale. 2019;11:14032–41. doi: 10.1039/C9NR02560J

109. Tran K, Tawfik SA, Spencer MJS. Restoring piezoelectric properties in 2D zinc oxide nanosheets by surface modifications: implications for piezoelectric nanogenerators. ACS Appl Nano Mater. 2023;6:14767–76. doi: 10.1021/acsanm.3c02200

110. Zhang G, Liao Q, Ma M, Gao F, Zhang Z, Kang Z, et al. Uniformly assembled vanadium doped ZnO microflowers/bacterial cellulose hybrid paper for flexible piezoelectric nanogenerators and self-powered sensors. Nano Energy. 2018;52:501–9. doi: 10.1016/j.nanoen.2018.08.020

111. Sinha N, Goel S, Joseph AJ, Yadav H, Batra K, Gupta MK, et al. Y-doped ZnO nanosheets: gigantic piezoelectric response for an ultra-sensitive flexible piezoelectric nanogenerator. Ceram Int. 2018;44:8582–90. doi: 10.1016/j.ceramint.2018.02.066

112. Batra K, Sinha N, Goel S, Yadav H, Joseph AJ, Kumar B. Enhanced dielectric, ferroelectric and piezoelectric performance of Nd-ZnO nanorods and their application in flexible piezoelectric nanogenerator. J Alloys Compd. 2018;767:1003–11. doi: 10.1016/j.jallcom.2018.07.187

113. Batra K, Sinha N, Kumar B. Tb-doped ZnO:PDMS based flexible nanogenerator with enhanced piezoelectric output performance by optimizing nanofiller concentration. Ceram Int. 2020;46:24120–8. doi: 10.1016/j.ceramint.2020.06.191

114. Batra K, Sinha N, Kumar B. Ba-doped ZnO nanorods: efficient piezoelectric filler material for PDMS based flexible nanogenerator. Vacuum. 2021;191:110385. doi: 10.1016/j.vacuum.2021.110385

115. Hasan Z, Rahman MA, Das DK, Rouf HK. Influence of Ca doping in structural, electronic, optical and mechanical properties of $Ba_{1-x}Ca_xTiO_3$ perovskite from first-principles investigation. Sci Rep. 2023;13:10487. doi: 10.1038/s41598-023-36719-8

116. Zheng T, Wu J, Xiao D, Zhu J. Recent development in lead-free perovskite piezoelectric bulk materials. Prog Mater Sci. 2018;98:552–624. doi: 10.1016/j.pmatsci.2018.06.002

117. Zhuang Y, Li J, Hu Q, Han S, Liu W, Peng C, et al. Flexible composites with Ce-coped $BaTiO_3$/P(VDF-TrFE) nanofibers for piezoelectric device. Compos Sci Technol. 2020;200:108386. doi: 10.1016/j.compscitech.2020.108386

118. Maity S, Sasmal A, Sen S. Barium titanate based paraelectric material incorporated poly(vinylidene fluoride) for biomechanical energy harvesting and self-powered mechanosensing. Mater Sci Semicond Process. 2023;153:107128. doi: 10.1016/j.mssp.2022.107128

119. Khadtare S, Kumar A, Jung U, Sang C, Park J. Piezoelectric nanogenerator based on lead-free $BiFeO_3$:Sr perovskite. J Alloys Compd. 2022;926:166738. doi: 10.1016/j.jallcom.2022.166738

120. Sasmal A, Sen S, Devi PS. Role of suppressed oxygen vacancies in the $BiFeO_3$ nanofiller to improve the polar phase and multifunctional performance of poly(vinylidene fluoride). Phys Chem Chem Phys. 2019;21:5974–88. doi: 10.1039/C8CP07281G

121. Sasmal A, Sen S, Devi PS. Significantly suppressed leakage current and reduced band gap of $BiFeO_3$ through Ba–Zr Co-substitution: structural, optical, electrical and magnetic study. Mater Chem Phys. 2020;254:123362. doi: 10.1016/j.matchemphys.2020.123362

122. Sasmal A, Sen S, Devi PS. Frequency dependent energy storage and dielectric performance of Ba–Zr co-doped $BiFeO_3$ loaded PVDF based mechanical energy harvesters: effect of corona poling. Soft Matter. 2020;16:8492–505. doi: 10.1039/D0SM01031F

123. Zhang Y, Wu M, Zhu Q, Wang F, Su H, Li H, et al. Performance enhancement of flexible piezoelectric nanogenerator via doping and rational 3D structure design for self-powered mechanosensational system. Adv Funct Mater. 2019;29:1904259. doi: 10.1002/adfm.201904259

124. Shawon SMAZ, Carballo ZD, Vega VS, Lin C, Rafaqut MS, Sun AX, et al. Surface modified hybrid $ZnSnO_3$ nanocubes for enhanced piezoelectric power generation and wireless sensory application. Nano Energy. 2022;92:106653. doi: 10.1016/j.nanoen.2021.106653

125. Vivekananthan V, Chandrasekhar A, Alluri NR, Purusothaman Y, Kim WJ, Kang CN, et al. A flexible piezoelectric composite nanogenerator based on doping enhanced lead-free nanoparticles. Mater Lett. 2019;249:73–76. doi: 10.1016/j.matlet.2019.02.134

126. Paraknowitsch JP, Thomas A. Doping carbons beyond nitrogen: an overview of advanced heteroatom doped carbons with boron, sulphur and phosphorus for energy applications. Energy Environ Sci. 2013;6:2839–55. doi: 10.1039/C3EE41444B

127. Sarkar D, Das N, Saikh MM, Biswas P, Roy S, Paul S, et al. High β-crystallinity comprising nitrogenous carbon dot/PVDF nanocomposite decorated self-powered and flexible piezoelectric nanogenerator for harvesting human movement mediated energy and sensing weights. Ceram Int. 2023;49:5466–78. doi: 10.1016/j.ceramint.2022.10.070

128. Rana S, Singh V, Singh B. Tailoring the output performance of PVDF-Based piezo–tribo hybridized nanogenerators via B, N-codoped reduced graphene oxide. ACS Appl Electron Mater. 2022;4:5893–904. doi: 10.1021/acsaelm.2c01085

129. Ning W, Gao F. Structural and functional diversity in lead-free halide perovskite materials. Adv Mater. 2019;31:1900326. doi: 10.1002/adma.201900326

130. Guan X, Wang Z, Zhao W, Huang H, Wang S, Zhang Q, et al. Flexible piezoresistive sensors with wide-range pressure measurements based on a graded nest-like architecture. ACS Appl Mater Interfaces. 2020;12:26137–44. doi: 10.1021/acsami.0c03326

131. Giannattasio C, Vincenti A, Failla M, Capra A, Cirò A, De Ceglia S, et al. Effects of heart rate changes on arterial distensibility in humans. Hypertension. 2003;42:253–6. doi: 10.1161/01.HYP.0000085199.33254.15

132. Zhao C, Zhang Q, Zhang W, Du X, Zhang Y, Gong S, et al. Hybrid piezo/triboelectric nanogenerator for highly efficient and stable rotation energy harvesting. Nano Energy. 2019;57:440–9. doi: 10.1016/j.nanoen.2018.12.062

133. Kang CW, Lee DM, Park J, Bang S, Kim SW, Son SU. Core-shell ZnO@microporous organic polymer nanospheres as enhanced piezo-triboelectric energy harvesting materials. Angew Chem Int Ed. 2022;61:e202209659. doi: 10.1002/anie.202209659

134. Paranjape MV, Graham SA, Patnam H, Manchi P, Yu JS. Dopamine treated $SnO_2$/PVDF composite films for hybrid mechanical energy harvester. Compos Sci Technol. 2022;221:109323. doi: 10.1016/j.compscitech.2022.109323

135. Jin CC, Liu DM, Zhang LX. An emerging family of piezocatalysts: 2D piezoelectric materials. Small. 2023;19:2303586. doi: 10.1002/smll.202303586

136. Zheng H, Wang Y, Liu J, Wang J, Yan K, Zhu K. Recent advancements in the use of novel piezoelectric materials for piezocatalytic and piezo-photocatalytic applications. Appl Catal B Environ. 2024;341:123335. doi: 10.1016/j.apcatb.2023.123335

137. Pang F, Zhao P, Lee HY, Kim DJ, Meng X, Cho MY, et al. Progress and perspectives in 2D piezoelectric materials for piezotronics and piezo-phototronics. Adv Sci. 2025;12:2411422. doi: 10.1002/advs.202411422

138. Sun Y, Gao J, Cheng Y, Zhang YW, Zeng K. Design of the hybrid metal–organic frameworks as potential supramolecular piezo-/ferroelectrics. J Phys Chem C. 2019;123:3122–9. doi: 10.1021/acs.jpcc.8b08442

139. Shaukat RA, Saqub QM, Kim J, Song H, Khan MU, Chougale MY, et al. Ultra-robust tribo- and piezo-electric nanogenerator based on metal organic frameworks (MOF-5) with high environmental stability. Nano Energy. 2022;96:107128. doi: 10.1016/j.nanoen.2022.107128

140. Zhou X, Miao Y, Suslick KS, Dlott DD. Mechanochemistry of metal–organic frameworks under pressure and shock. Acc Chem Res. 2020;53:2806–2815. doi: 10.1021/acs.accounts.0c00396

141. Zhong J, Kankala RK, Wang SB, Chen AZ. Recent advances in polymeric nanocomposites of metal-organic frameworks (MOFs). Polymers. 2019;11:1627. doi: 10.3390/polym11101627

142. Soomro RA, Zhang P, Fan B, Wei Y, Xu B. Progression in the oxidation stability of MXenes. Nano-Micro Lett. 2023;15:108. doi: 10.1007/s40820-023-01069-7

143. Ding M, Cai X, Jiang HL. Improving MOF stability: approaches and applications. Chem Sci. 2019;10:10209–30. doi: 10.1039/c9sc03916c